UNIVERSITY OF TROMSØ UIT

FACULTY OF SCIENCE AND TECHNOLOGY
DEPARTMENT OF PHYSICS AND TECHNOLOGY

The University Centre in Svalbard

Department of Arctic Technology

Empirical and dynamical modeling of debris flow events close to Longyearbyen and Svea, Svalbard

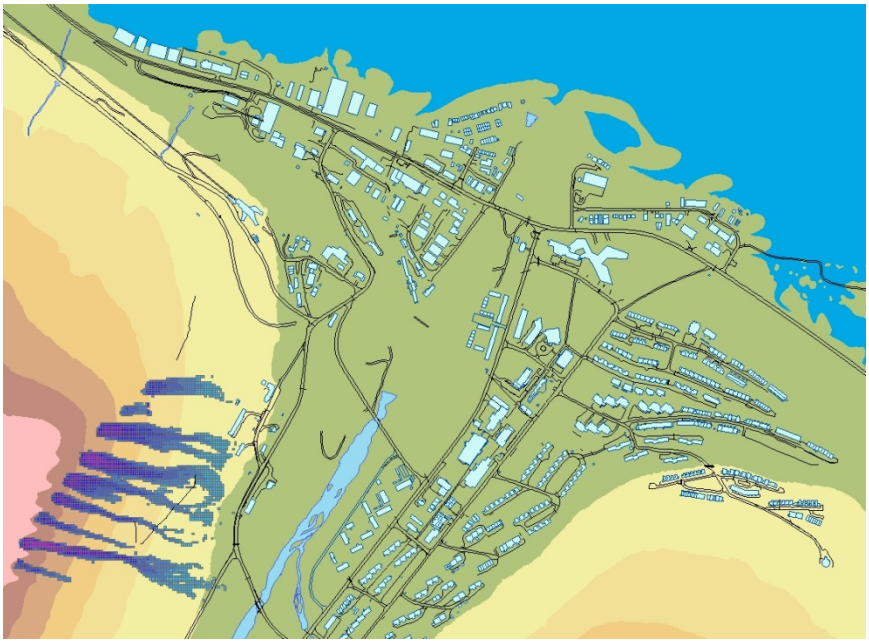

Christian Engelke

06/2011-06/2012 TEK-3900
Master's thesis in Technology and Safety in the High North

June 2012

Sammendrag

Mens flomskred er relativt godt studert i tett befolkede fjellområder, er det få undersøkelser som har blitt gjennomført i arktiske regioner med permafrost. For å få en bedre forståelse av prosessene som er involvert i et slikt miljø, fokuserer dette arbeidet på flomskred i fjellene i nærheten av Longyearbyen og Svea på Svalbard, Norge, som ligger på 78°N.

Totalt ble 52 flomskred undersøkt i dette arktiske området mellom juli og oktober 2011. Den innsamlede informasjonen om flomskredene ble kombinert med svært nøyaktige kartdata for å få bakkeprofiler. Disse profilene ble brukt til både empiriske og dynamiske modelleringer av utløpet til flomskredene.

Empirisk modellering viste at αβ- og NGI-modellen, som begge er kalibrert for fastlandet, kunne brukes for å få en bedre forståelse om maksimalt utløp av flomskredene. Generelt passer resultatene av αβ - modellen og NGI modellen til de målte maksimale utløpene.

Likevel viste de Svalbard-kalibrerte modellene en viss grad av forbedring i nøyaktighet. Til ingeniørtekniske formål ble lineare regresjoner for de lengste utløpene gjennomført, og modellene basert på disse regresjonene kan brukes i evalueringer av eventuelle byggeplasser. Modellen som antar startprosessen av deponering på en vinkel av 20° oppnådde de beste resultatene med et standardavvik på 2.09°. Denne modellen anbefales til bruke for fremtidige evalueringer.

Den dynamiske modellen RAMMS er et flott verktøy for å finne flomskredets retning, men utløpet er vanskelig å anslå med programmet.

Abstract

Debris flows are a mountain slope hazard relatively well studied in densely populated mountainous regions, while few investigations have been done in Arctic permafrost regions. In order to get a better understanding of the processes involved in such an environment, this work focused on debris flow hazards in the mountains close to Longyearbyen and Svea on Svalbard, Norway, situated at 78°N.

A total of 52 debris flows were investigated in this Arctic environment between July and October 2011. The gathered slope information was embedded in highly accurate map data of the regions in order to get slope profiles of the debris flows. Those profiles were used for both empirical and dynamical modeling of the debris flow runout.

Empirical modeling showed that the mainland-calibrated αβ - model and NGI model may be used in order to get a better understanding about maximal runout of debris flows. In general, the output of the αβ – model and the NGI model fit the measured maximal runout.

Yet, Svalbard-calibrated models show a certain degree of improvement in accuracy. For engineering purposes, linear regressions for the longest runouts were performed. The models based on these regressions are advised to use for the evaluations of possible construction sites. The model assuming a deposition start angle of 20° achieved the best result with a standard deviation of 2.09°. This model is advised to use in future construction site planning.

The dynamical model RAMMS is a great tool for finding directions, although debris flow runouts are hard to estimate with the program.

Acknowledgements

The process of writing the thesis has been a very exciting experience, especially during the practical periods out in the field. I learnt a lot about mountain slope hazards in general, about meteorology, geology and of course about debris flows.

Thanks to the University Center in Svalbard for a great year and practical support during my stay. It was both scientific and personal a great experience to study another year at UNIS.

First and foremost I want to thank Prof. Jan Otto Larsen for supervising my thesis. The discussions, comments and lectures increased my knowledge by far.

I would also like to thank Marc Christen from WSL Institute for Snow and Avalanche Research SLF for his help with operating and understanding the dynamical modeling tool RAMMS.

Øyvind Skeie Hellum is acknowledged for his great assistance with ArcGIS.

Sincere thanks to Jaap van Rijckevorsel for a great time conducting fieldwork together.

Thanks to Morgan Bender, Amanda Goss, Mathilde Le Moullec and Helene LoCascio Sætre for proof-reading the thesis.

Last, but not least, I am indebted to Hanna Lindvall and Tim Dunker not only for proof-reading, but for supporting me a lot on the way to finishing the thesis.

Table of Contents

1 Introduction

Debris flow is a flow of sediment and water mixture in a manner as if it was a flow of continuous fluid driven by gravity, and it attains large mobility from the enlarged void space saturated with water or slurry (Takahashi 2007).

1.1 Background

Debris flows have been observed since ancient times, despite the fact that relatively little scientific work has been done about them. The mechanisms behind the transport of large boulders have not been investigated before the late 1960s. Since then there has been both theoretical and experimental research especially in Japan, leading to a deeper understanding of the physics behind the phenomena. Yet, debris flows are still less present in public than other mountain slope hazards, such as snow avalanches and landslides (Takahashi 2007).

As other mountain slope hazards have similarities to debris flows in aspect of their physical behavior, research in those fields gives positive side-effects to debris flow research, and vice-versa. For instance, in the last years a special focus has been put on 3D modeling for predicting and preventing snow avalanche disasters. This work is leading to improved models like the Austrian Elba or the Swiss RAMMS, which also include additional applications for debris flows.

In Norway, where the population is less dense than in the Alps or the Japanese mountain regions, historically there has been less knowledge about snow avalanches and debris flows. Yet, in the last years there has been research focus on snow avalanches, landslides and debris flows. This was, for instance, leading to the empirical αβ - model and the NGI model (Norges Geotekniske Institutt), predicting the runout of snow avalanches, respectively debris flows, and calibrated for the Norwegian mainland (Norem and Andersen 2011).

1.2 Debris flows on Svalbard

Svalbard is an Arctic archipelago administrated by the Norwegian state. This project investigates debris flows close to two Norwegian settlements Longyearbyen and Svea on Svalbard. One example of a debris flow channel close to the triggering zone situated at Haugen in Longyearbyen can be seen in Fig. 1. In addition there are several runouts situated close to the buildings down the slope.

Figure 1: Triggering zone close to Haugen (Picture: Christian Engelke, August 2011)

While there is an ongoing project in order to map and understand the risks of snow avalanches around the Norwegian settlement of Longyearbyen (Eckerstorfer et al. 2008), research on debris flows in Arctic environments has not been performed within the last 10 years.

Yet, several rainstorms leading to debris flows have shown that debris flows and related hazards may pose considerable risk to houses, buildings and people. For instance, big debris flow events took place on the July 10/11, 1972 and August 4/5, 1981. Additionally, there was a big slush flow in Vannledningsdalen on June 11, 1953 with three fatalities. Stig Larsson has mapped the debris flows of the 1972 event. He found out that around 7000m^3 of debris was eroded in a catchment area of 6,8km^2. Just before those slope failures a rainstorm with 31mm of precipitation within 12h was recorded. Thus heavy rainstorms have significance for the erosion of Svalbard slopes. Larsson also claimed that a future increase of precipitation will lead to more frequent debris flow events. Fig. 2 shows a map with some of the debris flows from the incident at Haugen and around the old town center of Longyearbyen (Larsson 1982).

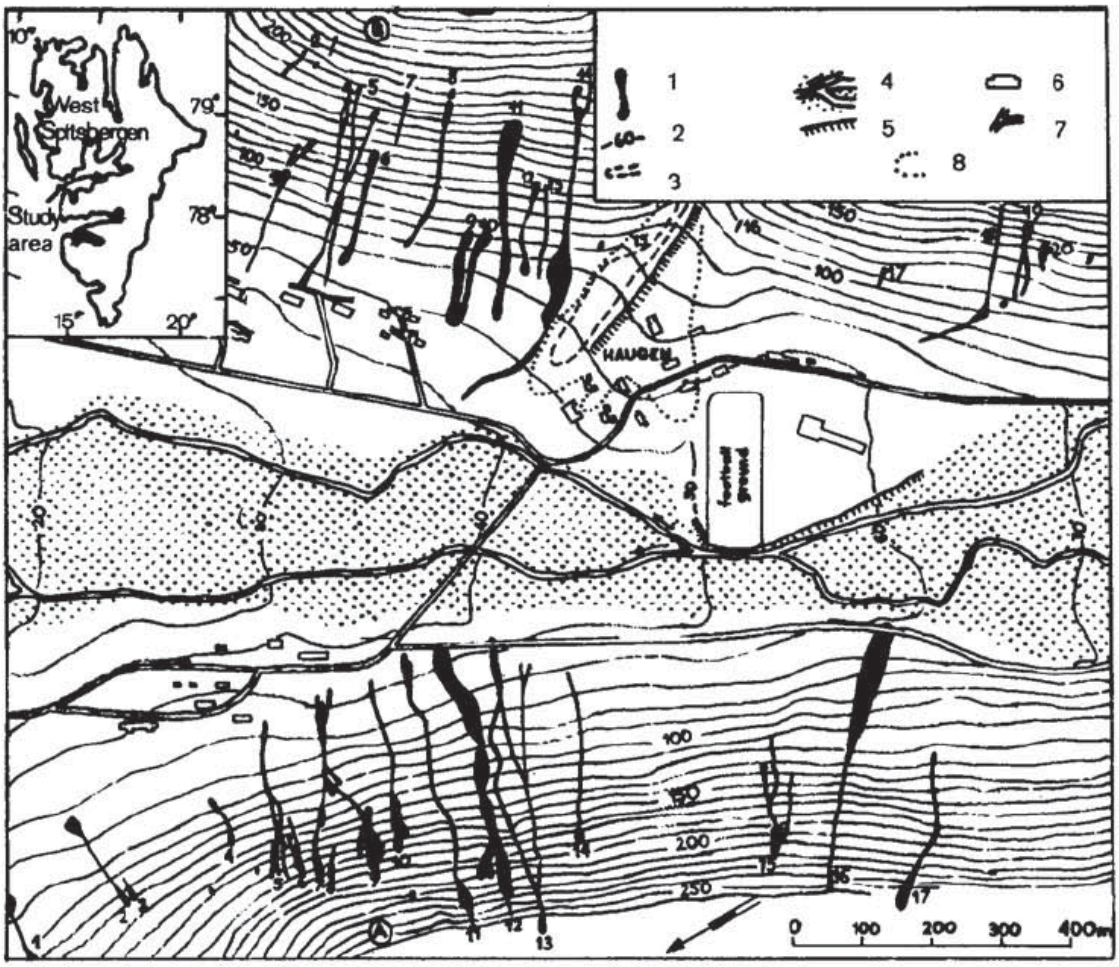

Figure 2: Old debris flows from the rain storm of July 1972 on the Northern side of Longyeardalen (Larsson 1982)

1.3 Project idea

The aim of this work is to gain further knowledge about the characteristics of debris flows on Svalbard and through this receive a better understanding of the risk of debris flow hazards on Svalbard

The first part of this work is the mapping of past debris flows in several valleys close to Longyearbyen (Longyeardalen, Bjørndalen and Endalen) and close to the mining community Sveagruva. The main focus is on Longyeardalen, as most debris flows are in this valley and risk to people is evident here. This work includes reinvestigation of debris flows examined by Stig Larsson, but also from other incidents over the last decades that are not investigated, yet. Center of attention is the maximal runout and its relation to the slope angles in the profile of the flows.

Secondly, the results of the fieldwork are compared to model-outputs from both, the Norwegian αβ - model, the NGI (Norges Geotekniske Institutt) model and the Swiss

RAMMS (rapid mass movements) model. These models are explained with further information later on both in terms of mathematical background and physical behavior.

The three models all have to be calibrated for Svalbard conditions and will be evaluated with regards to their practicability. Also possible differences to mainland conditions are investigated.

A summary with the main conclusions and some thoughts of how to further develop this work are presented in the final part of the report.

2 Theory

2.1 Location

Figure 3: Map of the Svalbard archipelago (TopoSvalbard 2012)

Svalbard is an archipelago on the margin between the North Atlantic Ocean and the Arctic Ocean, situated between 74° N and 81° N latitude and between 10° E and 35° E longitude. Spitsbergen is the largest island of the archipelago and all settlements are situated on this island. Longyearbyen is the administrative center and biggest settlement of Spitsbergen. Sveagruva is a mining city lying around 60km south of Longyearbyen.

2.1.1 Climate

The climate with its three main factors being temperature, precipitation and wind, plays the key role considering the formation of any kind of avalanche. Models for mountain slope hazards are therefore built up on climate models (McClung and Schaerer 2006).

Mountain slope hazards are often directly linked to precipitation. While snow fall is obviously linked to the formation of snow avalanches, rain or melting snow might result in slush flows, debris flows or landslides. Debris flows are normally linked to heavy rainstorms and/or rapid snow melt (Takahashi 2007).

Svalbard conditions

Typical for an Arctic climate are low temperatures, dry air and low rates of annual precipitation.

Svalbard has a relatively maritime Arctic climate. Between 1961 and 1990, Svalbard airport had a yearly average temperature of -6.7°C and 190mm of precipitation. The more maritime Ny-Ålesund had averages of -6.4°C and 370mm in the same period (met.no 2012). For its latitude, especially the western coast of Svalbard is relatively warm, as shown in Fig. 4. This is due to the warming effect of the North Atlantic Drift resulting in the West Spitsbergen current. While more than 60% of Svalbard is covered with glaciers, Nordenskiöldland, which is the peninsula where Longyearbyen and Svea are situated, is relatively free of glaciers (Elvevold et al. 2007). After the commonly used climate classification of Köppen, Svalbard is lying in the climate zone ET (tundra climate). This means that all months have an average temperature below +10°C, while the warmest month is having an average temperature between 0°C and +10°C (McKnight and Hess 2000).

In addition, the fact that there are four months of darkness and four months of midnight sun is an interesting astronomic detail with climatic effects. Midnight sun conditions may influence snow melting and the debris flow season due to steady melt and lack of refreeze in the nights (Humlum et al. 2003).

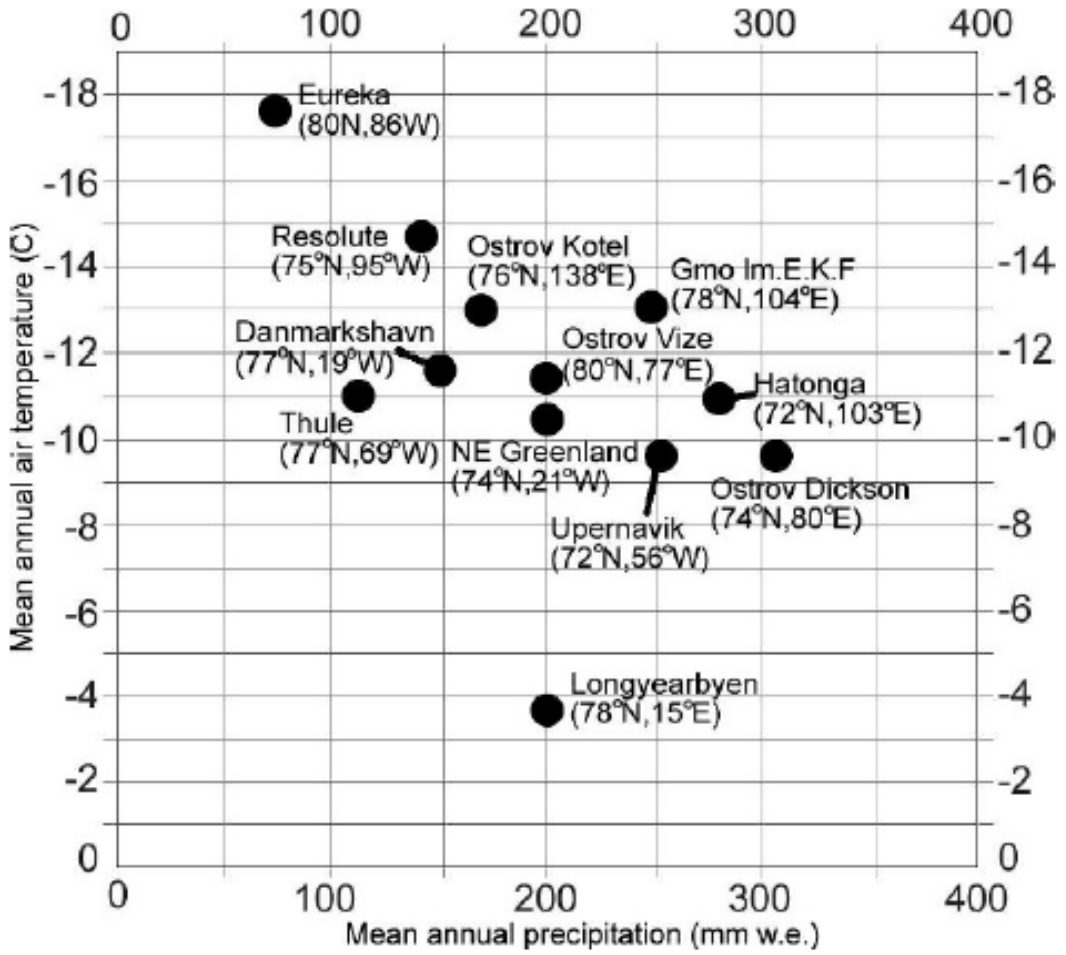

Figure 4: Mean annual temperature and precipitation for 2011 (data from http://www.climate-charts.com and http://www.wunderground.com). All stations are situated below 100 meters above sea level.

Permafrost

The negative mean annual air temperature is the reason for the permafrost formation. The permafrost depth around Longyearbyen is between 100m and 200m, and the active layer (the uppermost part of the permafrost which melts in summer) is between 1.0m and 1.5m. When comparing Svalbard to other regions, for example mainland of Norway, it is important to remember the presence of permafrost which might lead to a difference in ground behavior and thus a variation in mass movement processes (Pedersen and Hellum 2007).

Climate change effects

The effect of climate change will additionally complicate the conditions on Svalbard. Even if the permafrost around Longyearbyen is relatively warm, the immediate danger of decomposition of the permafrost is not yet existent. Still an increase of several degrees will lead to a deeper active layer and higher precipitation. This will favor the occurrence of all types of avalanches (Solomon et al. 2007).

Higher precipitation rates on Svalbard were already recorded between 1934-1975 (Åkerman 1980) and the trend continues according to recent research (IPCC-AR4-WG1 2007). As strong rainfall plays the key role in debris flow occurrence, these facts have to be considered for estimating future risks (Larsen 2005).

2.2 Mountain slope hazards in general

Considering mountain slope hazards snow avalanches most readily come to mind, as they are well covered in media and general public attention. Yet, there is a wide spectrum of mountain-slope hazards such as debris flows, rockfall and landslides. As people in mountainous regions are most aware of those hazards, knowledge is mainly based on observations from alpine regions, such as the Alps in central Europe, the Rocky Mountains in the USA and Canada, and the densely populated mountain regions of Japan. As often in history, big disasters have led to increased research. One example is the “winter of terror” in the central and Eastern Alps in 1951. During this winter a previously unrecorded number of avalanches took place in the Swiss and Austrian Alps mostly due to heavy snowfall. The series of 649 avalanches killed over 265 people. Past 1951, increased research activities have been conducted, leading to more reforestation and increased adoption of avalanche dams and fences (Haid 2007).

Mountains slope hazards are both a threat to people and to infrastructure such as streets and buildings. In Western Canada, for example, there are on average 12 fatalities and 10 million USD are invested in avalanche control and safety programs every year (McClung and Schaerer 2006).

As there is an increase of human activities in mountainous regions, disasters that were formerly unknown in certain areas are coming into the focus. Towns are spreading up mountain slopes, roads are built over new passes and mountain forests are logged in favor of farmlands.

2.2.1 Definition of avalanches

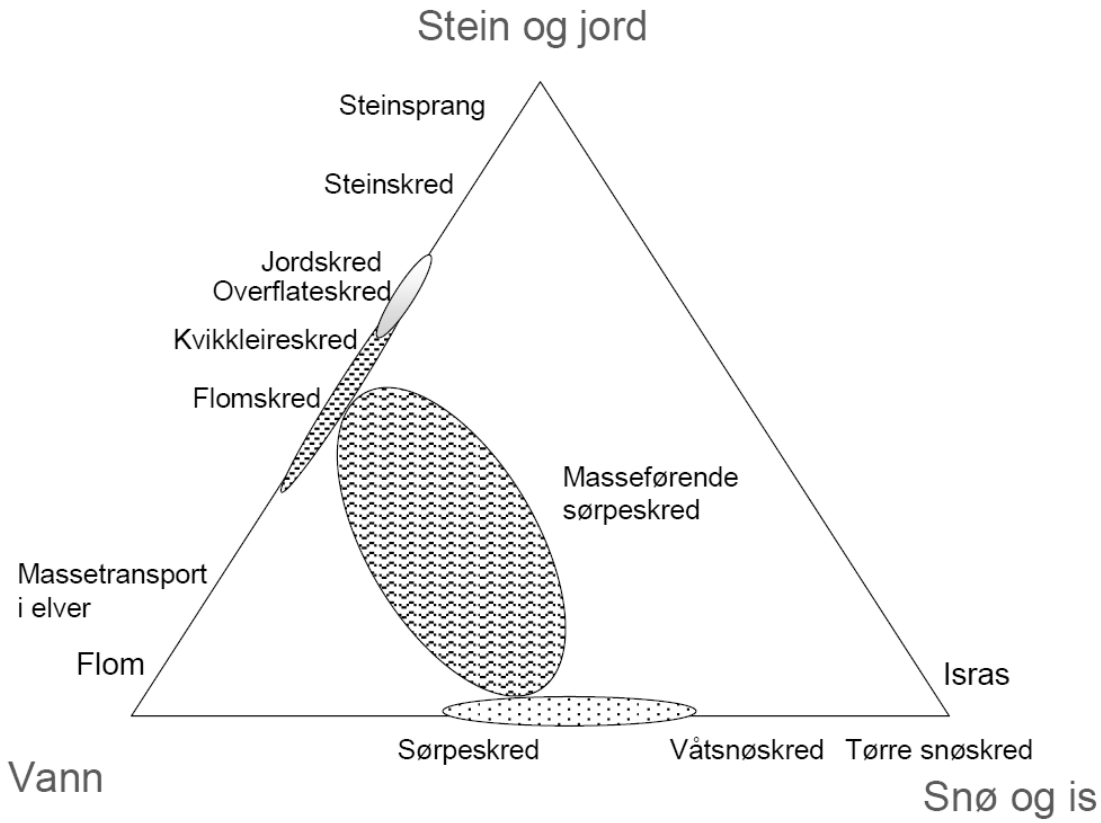

Figure 5: Triangle diagram for classification of avalanches (Norem and Andersen 2011).

There are several different ways to classify avalanches. Avalanches can be defined as a transport of masses such as snow, stone and soil including a certain degree of water. In addition avalanches might involve a certain amount of organic material such as trees or plants.

One example for classifying avalanches is a triangle diagram, see Fig. 5. Completely dry snow avalanches, rock fall and a river are representing the three pure avalanche types and thus the corners. Every other mass transport is a mixture of those different elements. The top corner of the triangle represents pure stone/soil avalanches; the bottom left corner represents pure water; the bottom right corner represents dry snow/ ice. In between are natural avalanches, such as debris flows or snow avalanches situated, representing a mixture of these three ideal type avalanches (Norem and Andersen 2011).

The amount of water is an important factor in determining the behavior of the mass transport. While rivers follow hydrodynamic characteristics, dry avalanches follow granular laws. Avalanches consisting of both dry parts and water follow a combination of both processes.

2.2.2 Snow avalanches

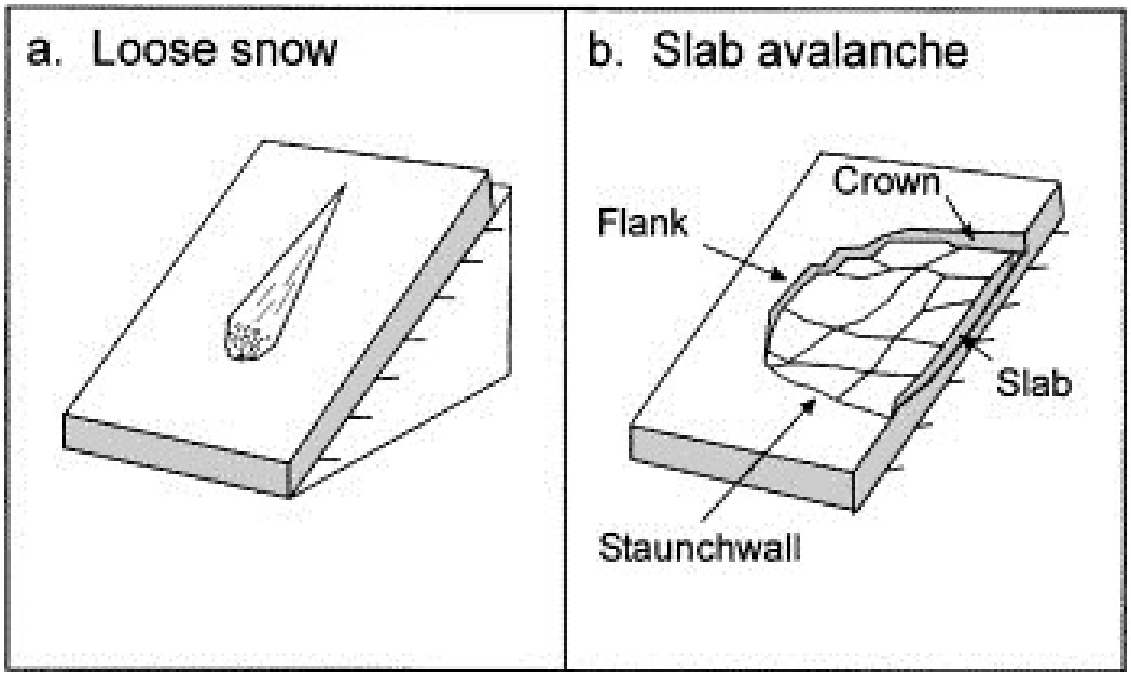

Figure 6: Draft of a loose snow avalanche (a) and a slab avalanche (b) (Reynolds 1992)

Snow avalanches can be divided into two types. Loose-snow avalanches usually involve near-surface snow and develop triangularly down a slope from a starting point as more and more snow is entrained into the slide.

Slab avalanches, though, are triggered by shear force on a weak layer within the snow pack, resulting in a collapse of a block of snow.

Usually, slab avalanches are more dangerous as they may involve hard snow layers under the surface. The draft of the two types in Fig. 6 shows the depths of the slab at both the crown and the flank of the avalanche (McClung and Schaerer 2006).

2.2.3 Rockfall

The phenomenon of single or multiple stone blocks moving down a slope is called rockfall. The volume of that event is maximum 100m^3, and thus relatively small (Broch and Nilsen 2001).

Rockfalls are initiated by weathering processes. In snowmelt or rainfall, water fills up cracks which are later widened due to freeze extension. Especially in spring and fall those freeze/thaw-rhythms occur relatively often. In the Svalbard climate those processes are reasonably active due to long periods with temperatures around the freezing point. In addition the lack of vegetation favors the occurrence of rockfalls.

Rockfalls can also be indicators for future landslides (Prick et al. 2004).

2.2.4 Rock avalanches

If the material involved in a rockfall exceeds some 100m^3 (up to 100.000m^3), it is defined as a rock avalanche. The blocks with the biggest mass will have the longest runout due to their higher kinetic energy (Dorren 2003).

2.2.5 Landslides

Landslides consist of even more material than rock avalanches and are typically related to high water content. When the soil is saturated with water, a lack of static friction within the mass occurs and the gliding process starts. Other trigger mechanisms of landslides might, for instance, be earthquakes (Highland and Bobrowsky 2008).

2.2.6 Slush flows

Slush flows have a similar physical behavior to debris flows that will be explained in Chapter 2.4. The difference between both types of flows is that slush flows consist of a high rate of snow while debris flows are mainly made up by stones and mud. Slush flows typically occur during rapid snow melt in spring time, or when heavy rainfall saturates the snow pack. The lack of drainage leads to saturation and the slush flow starts to move (Aryal and Sandven 2005).

2.3 Debris flows

As mentioned in 2.3.1, avalanches can be classified by their water content. Debris flows have water content between 30-70%, leading to a high mobility. In general, debris flows are triggered by intense rain falls or heavy snow melt. Furthermore, it is convenient to classify debris flows by the material involved and their physical behavior. Debris flows are larger than rockfalls, but smaller than landslides. The dimensions of debris flows are in the same range as rock avalanches but involve a different kind of material.

There are mainly three different types of debris flows; turbulent debris flows, viscous-type debris flows and stony-type debris flows. For a better understanding of the processes involved each of them is further described below.

Turbulent debris flow

Turbulent debris flows are characterized by high water content of ca. 70% and thus a low volumetric mass density. This type of debris flow is at the boundary to sediment transport in rivers. The typically very fine material with a diameter of less than 1mm in

diameter is transported by the turbulence of the stream. Turbulent flows can be calculated by classical hydrodynamic equations.

Viscous-type debris flow

Fully developed flows transport more material, leading to more friction between the particles, which attenuate the turbulence of the flow. Thus, the result is a continuous flow of particles and water. Erosion along the path of the flow involves larger particles, with particles above 10cm in diameter making up for as much as 50-70% of the mass. Viscous flows occur in surges, where the time scale between the individual waves, ranges from seconds to hours.

Stony-type debris flow

As with the viscous debris flow, the stony-type debris flow consists of a high mass density. These debris flow may involve huge boulders up to several meters (Takahashi 2007; Norem and Andersen 2011).

2.3.1 Tracks of debris flows

A typical debris flow track can be divided into three main parts with different characteristics. The classification between the erosional area, transport area and depositional area is shown in Fig. 7.

Mass transports often start with a small initial avalanche in areas between 20 and 45 degrees steepness which then triggers a lager avalanche. The uppermost steep part is referred to as the erosional area.

In the transport area which normally has steepness above 15 degrees, the flow increases in volume by involving sediments and eroding the landscape.

The depositional area with an angle of commonly below 15 degrees is characterized by flattening out or lack of channeling. Friction increases and the flow decelerates in this area (Hungr 2005).

Typically, there is boulder accumulation at the profile's head. There is also material aggregation on the sides of the debris flow channel, see Fig. 8.

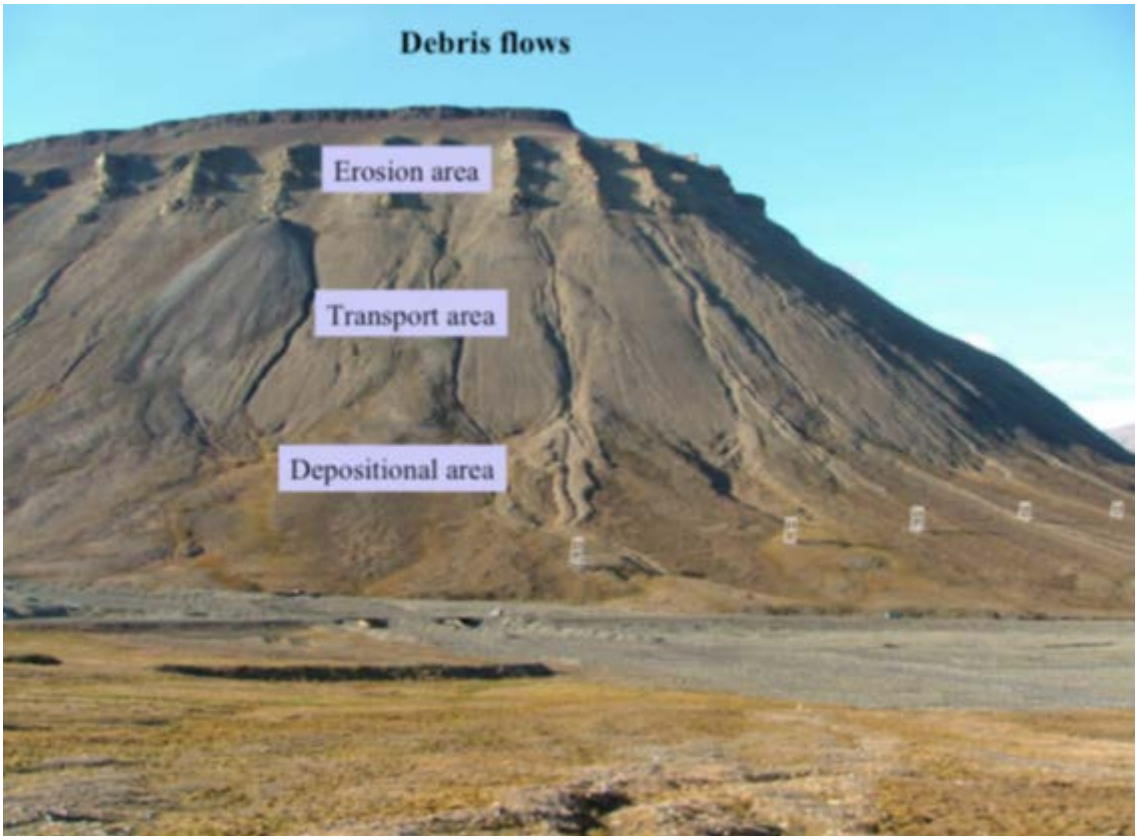

Figure 7: Debris flow track with erosion, transport and depositional area (Christiansen 2011)

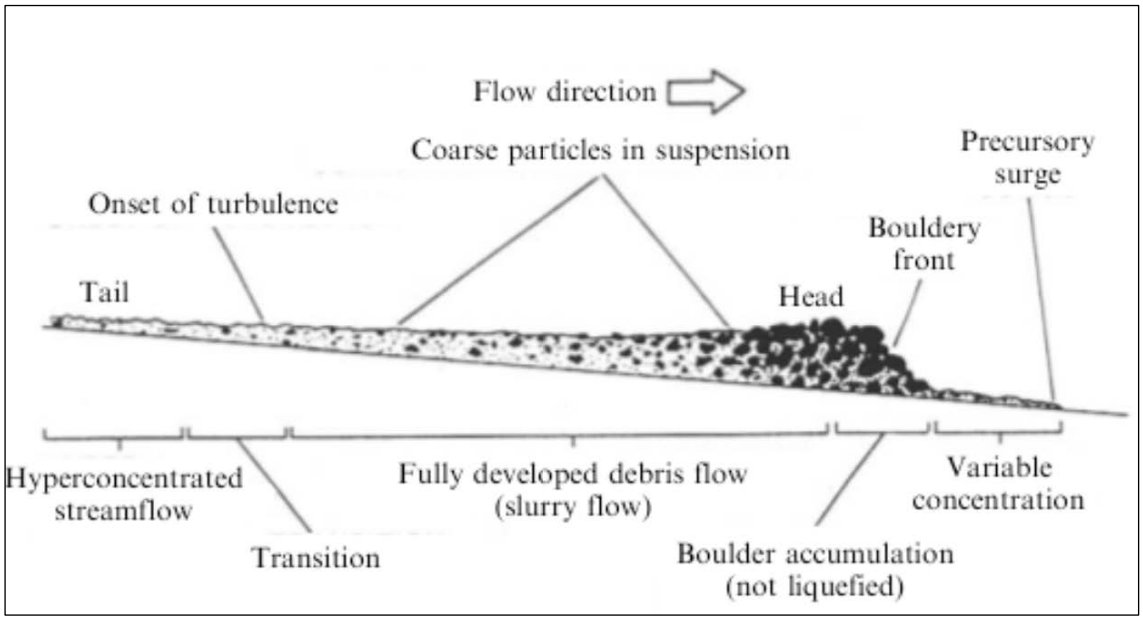

Figure 8: Debris flow movement profile (Hungr 2005)

2.3.2 Trigger mechanisms

Debris flows are triggered when the water content is high enough to saturate the masses. In general, debris flows are therefore triggered by strong rainfall and/or snowmelt. Additional water can also be supplied by groundwater accumulation, melting in rapid succession of volcano eruptions or drainage failures (NOAA-USGS 2005; Highland and Bobrowsky 2008). In this work only snowmelt and rainfall are considered as trigger mechanisms as these relate to Svalbard conditions.

Short and intense rainfall is generally not sufficient in order to saturate the ground material as it preferably erodes the surface layer and runs off as surface flow. Yet, long periods of steady water supply followed by heavy rainfall favor the occurrence of saturation of deeper lying layers. Physically, saturation leads to a reduced shear strength and thus the masses are more vulnerable to failure (Chatwin et al. 1994; Wieczorek and Glade 2005).

Fig. 9 shows the critical threshold correlation between the amount of precipitation and the period of precipitation, according to investigations of Caine in 1980. The same relation is found in equation (1). This threshold is the lower limit where one can expect the occurrence of avalanches (Lied and Bakkehøi 1980):

$$R = 14{,}82 \times D^{0{,}61} \qquad \text{(For 10min<D<240min),} \qquad (1)$$

where R = Amount of precipitation in mm within the precipitation period

D = Precipitation period in h (Caine 1980)

Another possibility to describe the criticality of debris flows is to use the function of the percentage of water supply over the last day in relation to a 100 year rain event over the saturation level of the ground. This relation is shown in Fig. 10.

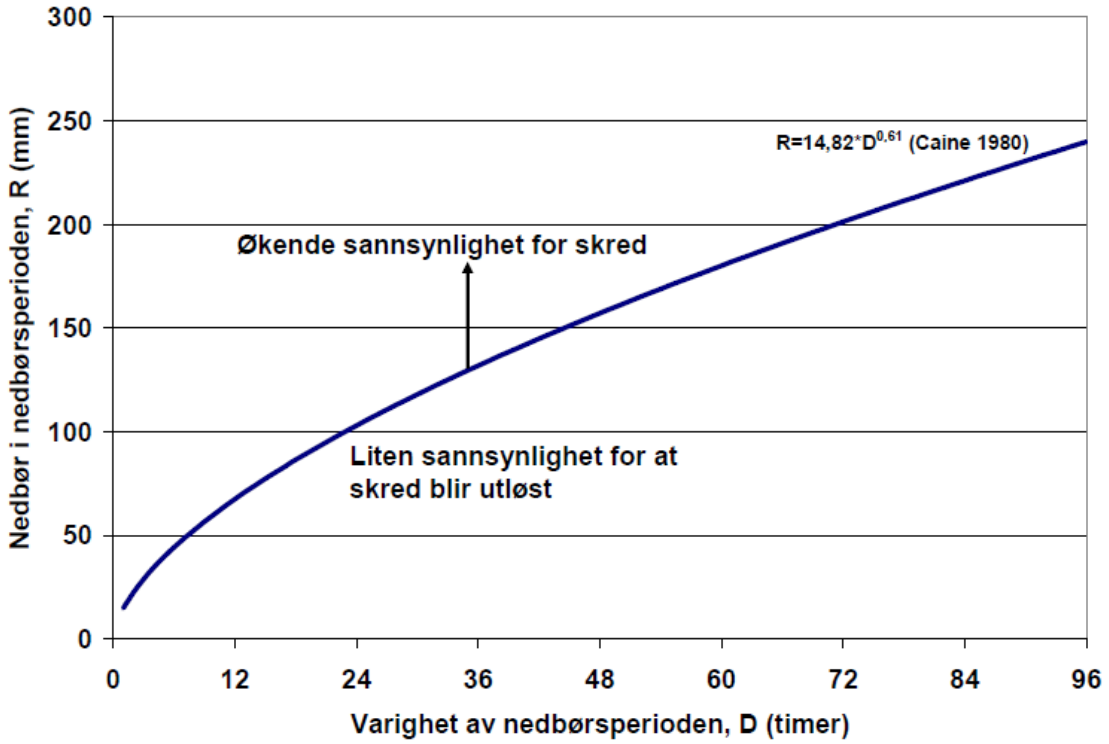

Figure 9: The critical threshold correlation between precipitation R, and precipitation period D (Caine 1980)

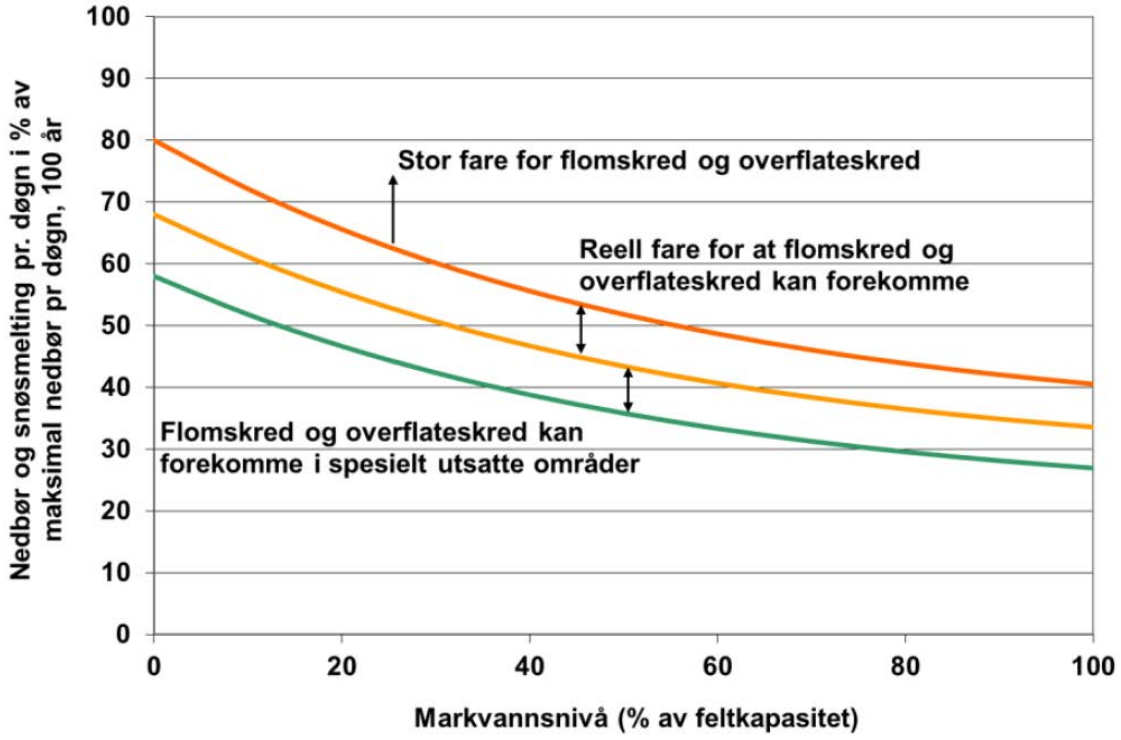

Figure 10: Danger of debris flow occurrence as a function of water supply in percentage of a 100 year rain event over ground saturation (Norem and Andersen 2011)

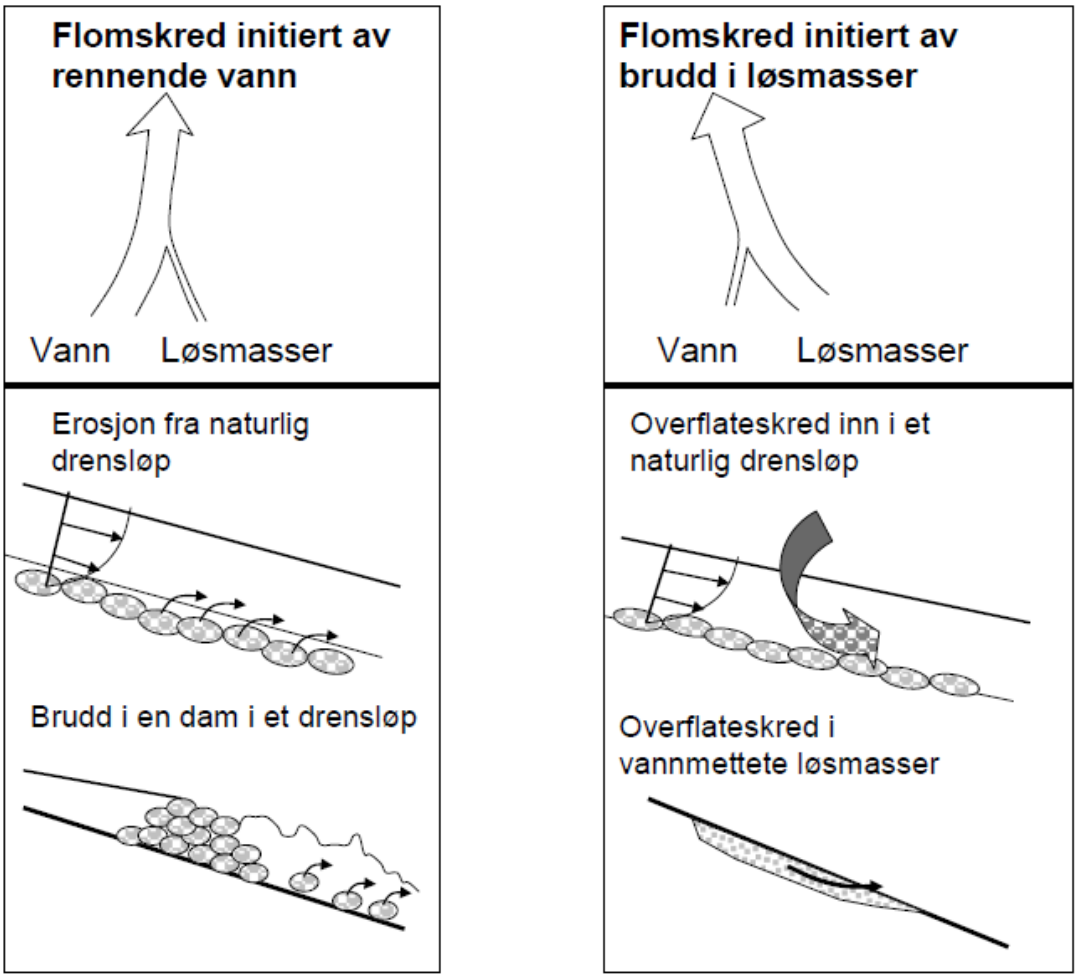

Figure 11: The two main initiation processes of debris flows (Norem and Andersen 2011)

Generally two types of initiation processes of debris flows are distinguished:

Debris flows can be initiated by running water which takes up loose material, or by a failure in the ground material. This is drafted in Fig. 11.

2.3.3 Runout of debris flows

There are different definitions about the runout of avalanches in general and debris flows in particular. The biggest part of the masses is deposited on the avalanche track, while parts are running further to the maximal runout. This is drafted in Fig. 12 (Legros 2002).

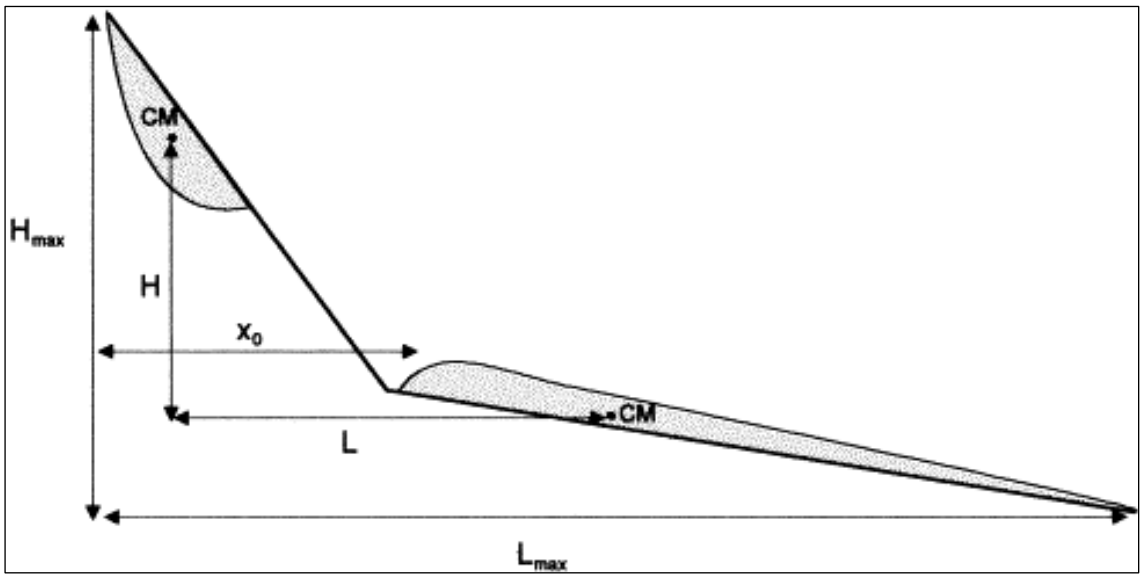

Figure 12: Sketch of landslide deposit and failing mass and definition of the parameters x_0, H, L, H_{max} *and* L_{max}. *CM indicates the center of mass of the failing mass and the deposit (Legros 2002).*

Yet, it has disadvantages to use either the center of the mass, CM, or maximal runout L_{max} as a value to measure the danger of debris flows. Obviously there is still a big damage potential below CM, as 50% of the masses are not deposited, yet. L_{max} is giving a very conservative value, though. As there is always high water content involved in debris flows, sediments will be transported by the flow far below the visible maximal runout. If this is taken into account, unrealistic high values for the runout are assumed. Therefore several publications suggest segmenting the runout zone according to deposition type and thus danger potential (VanDine 1996; Prochaska et al. 2008).

When designing in accordance to avalanche danger, one cannot expect to be prepared for all kind of avalanche events. The occurrence of extreme unforeseen events is always possible and avoidance of any risk is unrealistically restricting. It is therefore practical to define return periods of avalanche runouts as shown in Fig. 13. Acceptable return periods for different construction sites within a community have to be defined. In Norway, residential buildings, for instance, cannot be built within the 1,000 year period zone. The accepted return period of avalanches for streets, depending on the importance and the traffic appearance of the road, is between 20 and 50 years (Lied and Kristensen 2003b; Norem and Andersen 2011).

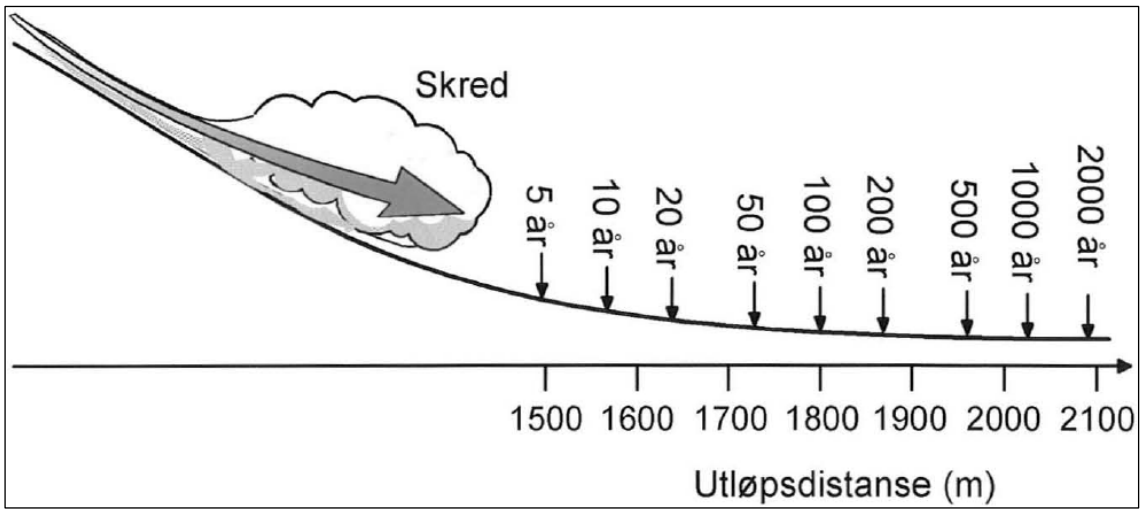

Figure 13: One way to categorize the size of an avalanche is by their return period (Lied and Kristensen 2003b)

Additionally, one has to take into account that avalanche runout typically increases with the volume involved. Runout also increases for material that has high water content and/or a large amount of fine grains. A sliding surface within the soil may also play an important role. Knowledge about those factors is absolutely necessary for the profound forecast of debris flow runouts (Norem and Andersen 2011).

2.3.4 Debris flow protection

There are numerous possibilities of protection against debris flows and other mountain slope hazards. Ditches, control ridges and fences are the most common way to secure an area. One of these methods can be seen behind the kindergarten at the western side of Longyeardalen, see Fig. 14.

The dimensions of the protection have to be chosen in order to fulfill the risk criteria according to the return periods named in 2.4.4. It is not economic to build, for instance, ridges that are constructed for a 1,000 year return period at a local road (Lied and Kristensen 2003b).

Figure 14: Trench, built in order to secure the kindergarten against snow avalanches and debris flows (Picture: Christian Engelke, September 2011)

2.3.5 Historical debris flow events on Svalbard

As mentioned in the introduction there were several large rainstorms in Svalbard history leading to debris flows. This shows that debris flows and related hazards may pose considerable risk to buildings and people, and communities.

The event of July 10/11, 1972 was profoundly investigated in 1982. Precipitation of 31mm within 12 hours, corresponding to 2.6mm/h was enough to trigger a huge amount of mountain slope failures in Longyeardalen. This value is a comparably low threshold to mainland Norway values. See Fig. 8 in 2.4.3, which proposes a 70mm threshold for slope failure for a period of 12 hours in mainland Norway (Caine 1980).

All debris flows of 1972 in Longyeardalen have been mapped, profiles have been plotted and the erosion volumes have been estimated. The research concluded that 7000m^3 of debris material was involved in a catchment area of 6,8km^2. This represents an average erosion, also called denudation, of 1mm (Larsson 1982).

Debris flows on Svalbard are small-scale events ranging up to several 100m^3 (André 1990). The biggest debris flow of the event of 1972 involved material corresponding to 800m^3 of volume. Slush flows may involve considerably bigger masses (Larsson 1982).

3 Methods

3.1 Fieldwork

In order to provide data about debris flows on Svalbard, measurements have been carried out at different sites throughout the autumn 2011. All field sites but one are closely situated to Longyearbyen, see Fig. 15. One location is at a slope close to Sveagruva, see Fig. 16.

In all 52 debris flows have been observed and mapped between August and early October 2011. In order to ensure high visibility, preferably days with clear weather and no precipitation have been chosen for observation.

As the focus within research has been on the runout of the debris flows, field work has focused on mapping these runouts. GPS coordinates and slope angles have been taken from the observed maximum runouts. The same data have also been taken for the start of the runout zone. If possible, the angels and GPS coordinates has also been taken from the triggering point. The success of collecting release area data has been dependent on the steepness and thus the danger of the slope.

For the measurement of the slope angle and distances an inclinometer and a laser distance measuring unit were used in the field. These instruments metered the distance and average slope angle from the runout to release area of the debris flows.

In addition, the material within the flow has been categorized qualitatively for size and age in order to get an idea of the water content and material transported by the flows. The water content can only be assumed by the composition of the material involved in the debris flows. The existence of fine grains is an aspect in favor of high water content, while huge boulders involved in the debris flows normally refer to low water content.

The size of erosional gullies and trenches was also recorded during fieldwork.

In cases where different generations of debris flows overlying each other exist, old mass movements have been disregarded in favor of taking young debris flows in the data sets. Indistinct flows have not been included in the dataset.

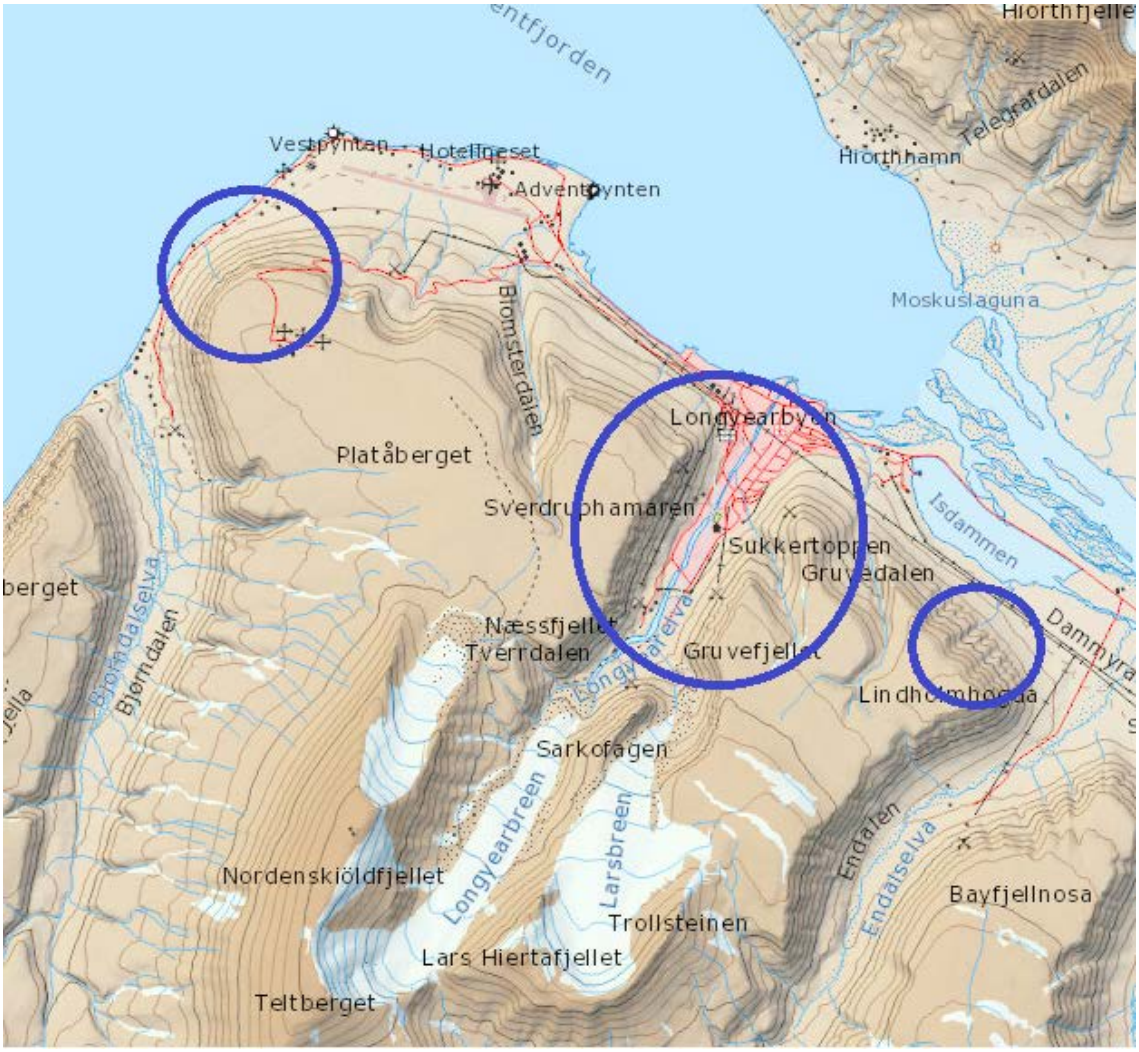

Figure 15: The field locations around Longyearbyen. From west to east: Bjørndalen, Longyeardalen and Endalen (TopoSvalbard 2012)

3.1.1 Longyeardalen

Most debris flows within this analysis are situated in Longyearbyen. There are several reasons for that. First of all, the main settlement Longyearbyen corresponds with an increased awareness of debris flows, danger and protection possibilities. In addition there is a high density of debris flows in most parts of the valley, especially at Haugen, at the old town center and in Nybyen. In all, 28 different distinctive debris flows have been chosen for the investigation in Longyeardalen. The field work has been carried out on several dates between August and October 2011.

3.1.2 Endalen

Measurements have been performed at the opening of Endalen towards Isdammen in late August 2011. Seven distinct debris flows have been observed and selected for further investigation at this field location.

3.1.3 Bjørndalen

In September 2011, field work between the airport and Bjørndalen has been conducted. Nine distinct debris flows have been chosen for further investigation, although many old, indistinctive debris flows were found in the area.

3.1.4 Sveagruva

Field work at Sveagruva has been carried out during two days in September 2011. Eight debris flows were investigated in this period.

At the time, the fieldwork has been conducted, it has not been clear yet, whether it would be possible to work with high resolution maps of the area of Svea afterwards. Therefore, in addition to the notation of the GPS coordinates at the run out, several GPS coordinates and angles have been taken within each single profile. This data has been acquired in order to get sufficient information about the profile of the debris flows, even without high resolution maps.

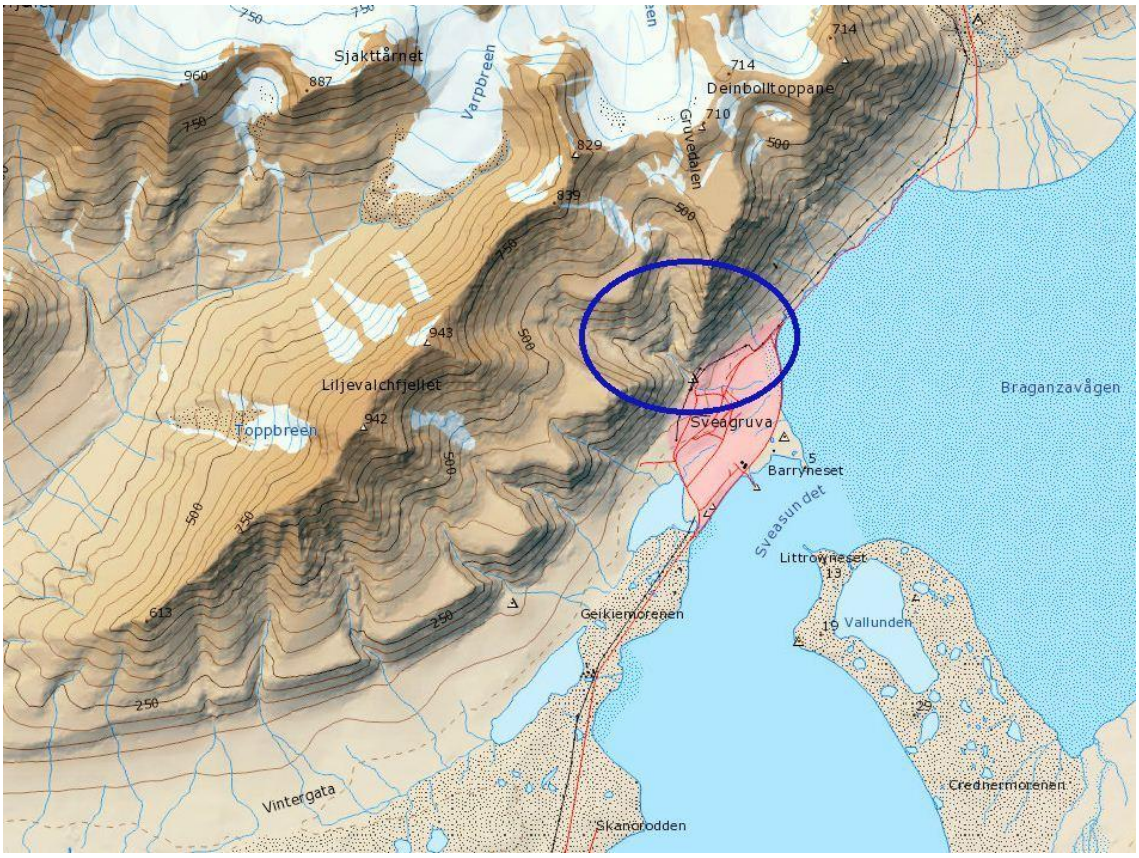

Figure 16: The field location at Sveagruva (TopoSvalbard 2012)

3.2 ArcGIS

ArcGIS is a geographic information system (GIS) which is an important tool within the working process. High resolution maps of Longyeardalen (1.0m resolution), Bjørndalen (5.0m resolution) and Endalen (5.0m resolution) are provided in .sos format by Bøye Bøland from Longyearbyen Lokalstyre. Bernt Holst from Store Norske Spitsbergen Kulkompani AS (SNSK) provided the project with maps (5.0m resolution) in the same format for Svea.

These maps in .sos format are transformed to a shape file which is readable by ArcGIS. Mistakes within the map data, such as wrong contour lines, are fixed before further work with the maps.

Afterwards it is possible to fit in the GPS data from the field into the map to illustrate the runout of the observed debris flows.

3.2.1 Debris flow profiles

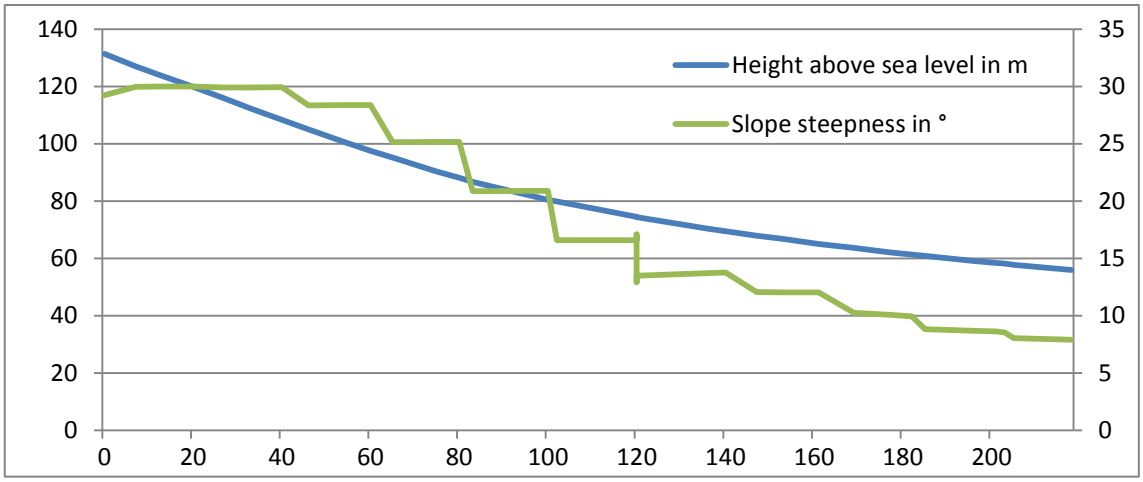

Figure 17: A typical "steepest path" generated profile, showing the slope distribution and the slopes steepness

With the tool "steepest path" it is possible to create profiles in the map that a natural avalanche would follow. If the map is detailed enough, this tool gives a lot better results than could ever be reached by measurements in the field.

Profiles are taken and analyzed for all 53 debris flows. A typical concave profile exported from ArcGIS can be seen in Fig. 17.

In some cases the "steepest path" tool did not work sufficiently and instead the tool "line of sight" was used to create similar profiles.

3.3 Modeling tools

For this project, the field data of the debris flows is compared with results of three different modeling tools to compare the different tools and how well they may predict the runout of debris flows. The dynamical RAMMS model is compared to the empirical αβ-model and the NGI model and all three models are evaluated. For linear regressions according to the different models the program OriginPro 8 is used.

3.3.1 αβ - model

Empirical models like the αβ - model or the NGI model are based on the profile of the avalanche track and on statistics about avalanches. Empirical models are not taking into account physical parameters like speed, material properties or friction parameters. Therefore they are relatively easy to use (Rickenmann 2005; Fannin and Bowman 2008).

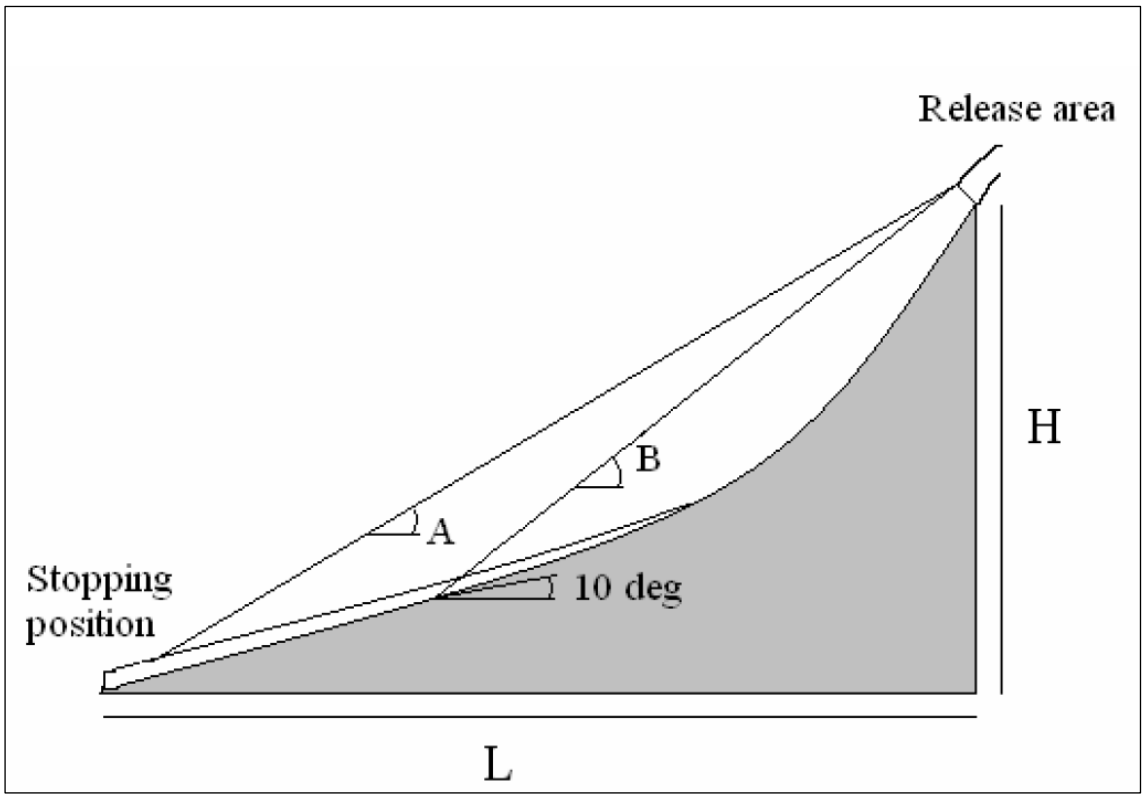

Figure 18: The avalanche profile showing the definition of the angles α and β for the αβ-model (Lied and Kristensen 2003a)

The αβ - model is originally calibrated with more than 200 snow avalanches from Western Norway (Lied and Bakkehøi 1980). It is defined that β is the angle between the release point and the point in the profile where the avalanche is starting to slow down. This point is assumed to be where the profile smoothens out to 10.0°. The idea behind the model is to describe the runout angle α as a function of β, see Fig. 18.

Regression analysis leads to formula (2) with a standard deviation (SD) of 2.3° (Bakkehøi et al. 1983):

$$\alpha = 0.96\beta - 1.4° \pm SD \quad (2)$$

3.3.2 NGI model

The NGI model is similar to the αβ - model, but assumes 20.0° instead of 10.0° steepness as the starting point for deposition, see Fig. 19. This takes into account the different behavior of debris flows compared to snow avalanches. (Norem and Andersen 2011).

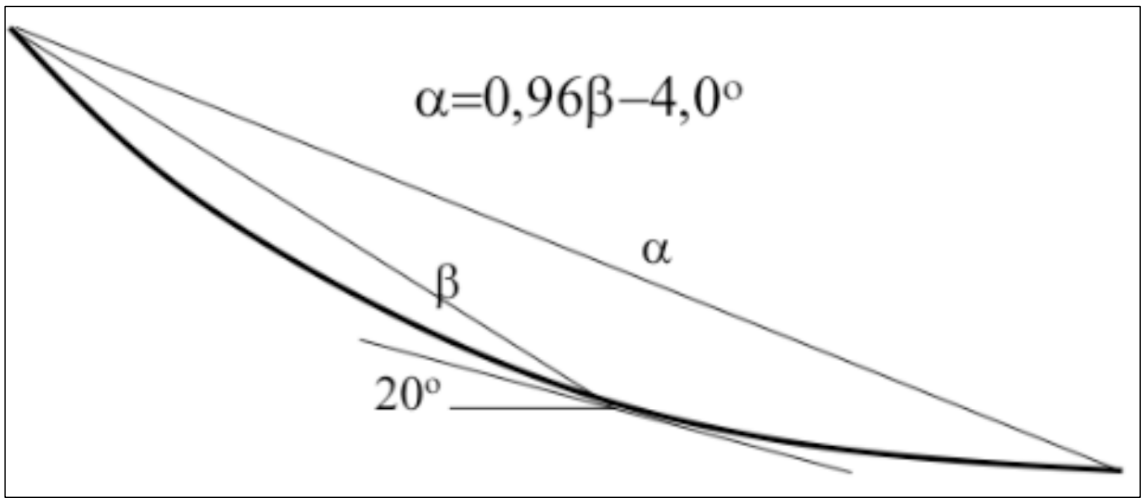

Figure 19: The definitions of the angles α and β according to the NGI debris flow model (Norem and Andersen 2011)

The model is calibrated for debris flows with low water content. The input data for the model is obtained from avalanches close to Forfjord on Vesterålen in Nordland, mainland Norway. The volume of the observed flows is between 2,000m^3 and 20,000m^3. Regression analysis leads to equation (3) with a standard deviation of 3.0° (Norem and Andersen 2011):

$$\alpha = 0.96\beta - 4.0° \pm SD \quad (3)$$

For the mapped debris flows in Norway, β varies between 23.0° and 30.0°, which leads to values for α between 18.1° and 24.8°. Compared to international research, these are relatively high values, corresponding to a short runout. This fact is most likely due to the smaller volume of the debris flows of the Norwegian research. Corominas, for instance, used debris flows and landslides between 10,000m^3 and 100,000m^3 for calibration of his model (Corominas 1996).

As Svalbard debris flows are of comparable small size, Corominas research is not taken into further account within this work.

3.3.3 Svalbard regression

In order to get the best correspondence for Svalbard, data from all debris flows is used for a linear regression simultaneous to the regressions from the mainland described in 3.3.1 and 3.3.2. Regressions are conducted with the 10.0°, 12.0°, 15.0° and 20.0° criteria for the start of deposition.

3.3.4 RAMMS debris flow

The physics behind the model

Dynamical models like the Swiss RAMMS or the Austrian Elba+ are taking into account physical parameters like speed, material properties, viscosity, avalanche volumes or friction parameters. In this work it is focused on RAMMS in disfavor of Elba+.

The physical model of RAMMS Debris Flow uses the Voellmy friction law. This model divides the frictional resistance into two parts: a dry-Coulomb type friction μ that scales with the normal stress and a velocity-squared drag or viscous-turbulent friction coefficient ξ. The frictional resistance *S(Pa)* is then

$$S = \mu\rho Hg \cdot cos(\phi) + \frac{\rho g U^2}{\xi}, \quad (4)$$

where ρ is the density, g the gravitational acceleration, ϕ the slope angle, H the flow height and U the flow velocity. The normal stress on the running surface, $\rho Hg \cdot cos(\phi)$, is summarized as a single parameter N.

The Voellmy model accounts for the resistance of the solid phase; μ is sometimes expressed as the tangent of the internal shear angle, and a viscous or turbulent fluid phase; ξ was introduced by Voellmy using hydrodynamic arguments.

RAMMS debris flow is calculated for release volume between 10,000m^3 and 100,000m^3 (RAMMS 2011).

Working scheme with RAMMS

In this work the version RAMMS Debris Flow 1.4.14 is used.

In practice first an ASCII File with topographic data from the different field sites is imported from ArcGIS. Afterwards single or different release areas are defined; see the colored polygons in Fig. 20. It is possible to define release volumes to every single polygon. In addition a calculation area is defined. This area can be seen as the green polygon around the colored release areas.

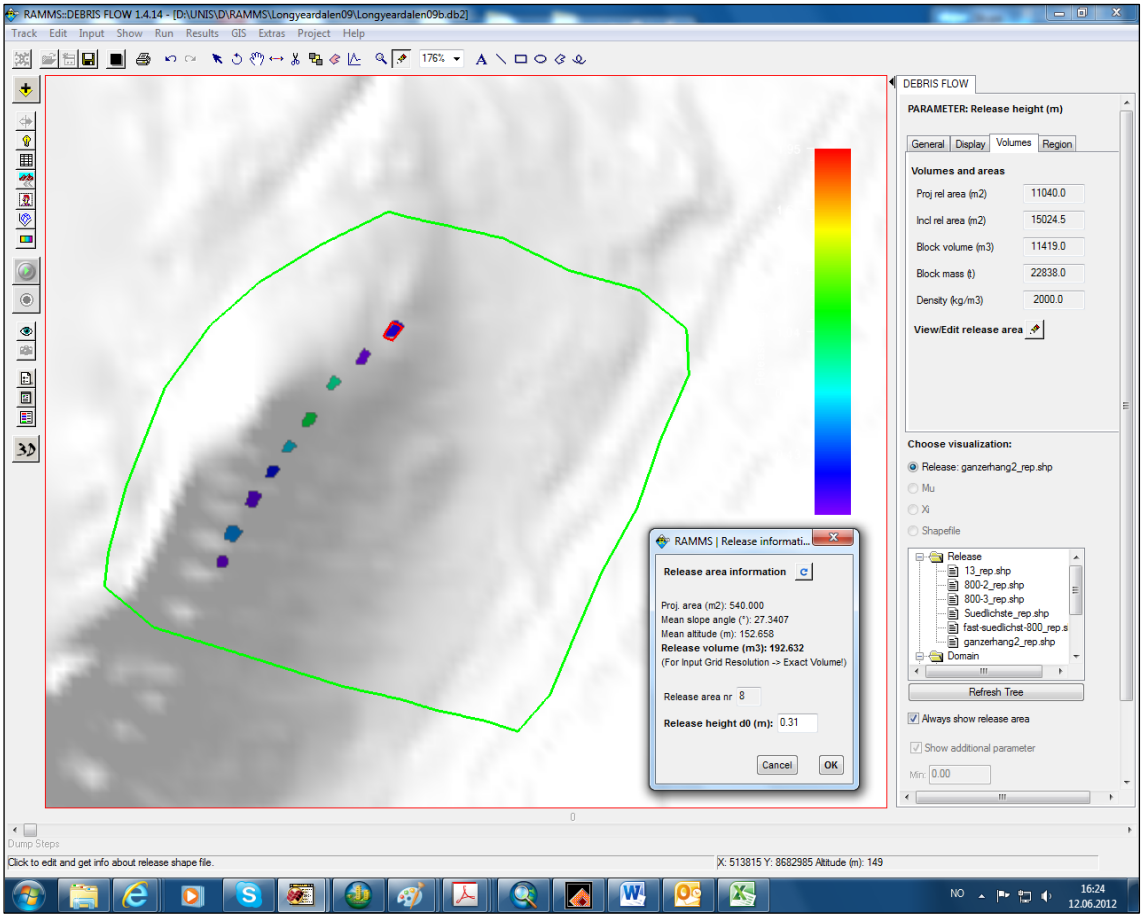

Figure 20: Drawing and defining of release areas and calculation domains in RAMMS Debris Flow

Before running the calculation, reasonable values for ρ, μ and ξ have to be chosen. The process is well described in the RAMMS User Manual (RAMMS 2011).

Before using RAMMS to achieve results about the runout of debris flows around Longyearbyen, first some calibrations have to be done. Results from the widely investigated debris flows from the 1972 rainstorm are compared to RAMMS results with different combinations of ρ, μ and ξ. Reasonable values with results fitting to the investigations of Larsson are used for further analyze.

RAMMS is giving results for the velocity, the flow height, the flow momentum and the pressure. When analyzing the data for the runout, it is focused on the results for the flow momentum. Due to numerical simulation patterns, the other runout results are always exaggerated (Christen 2012).

4 Results

In this section, results from fieldwork, and empirical and dynamical modeling with different models are presented.

4.1 Fieldwork

In this chapter the results from the surveys between August and October 2011 are presented. The blue dots in the figures are representing observed maximal runouts for historic debris flows, while the profiles in black and red/green are representing possible debris flow routes. The different colors in the map show different height levels, starting from lowlands painted in green, while higher levels are painted in dark brown. All maps are aligned to the north direction.

The black profiles correspond to results of the “steepest path” tool of ArcGIS, while the red/green profiles show the outcome of the tool “line of sight”. The debris flows are numbered, starting with 1 for every region. In the latter, the debris flows will be called Lyr01-28, End01-07, Bjo01-09 and Sve01-08 for distinguishing between the regions. Pictures of the different debris flows are shown in the Appendix B.

Most debris flows can be allocated to the class of stony type debris flows. Fine material at the runouts of End03-07, Bjo07-09, Lyr01, Lyr24-Lyr28 and Sve04-05 means these certain debris flows are most likely of the viscous type. Sve-04-05 might be of the turbulent flow type as very fine grains are involved.

The map data shows that the runout angle α is between 17.6° and 30.4° for all debris flows. The release area is observed to be between 24.0° and 42.1°.

4.1.1 Longyeardalen

Fig. 21 and Fig. 22 show respectively the north and south part of the Longyeardalen.

It is easy to observe that several debris flows are close to present buildings. That is especially the case around the church in the northwestern part of Longyeardalen (Lyr01-Lyr03) and at Haugen in the northeastern part of the valley (Lyr24-Lyr27). Buildings in Nybyen in the southeastern part of the valley (Lyr13-18) are also located close to past debris flows.

The material involved in the debris flows is fairly different. In the southern part of the valley, huge boulders up to 2.0m diameter are transported. The trenches are as deep as 2.0m and the stones above 0.10m in diameter make up 70% of the mass. In the northern

part of the valley at the old town and Haugen, this fraction is only about 40%. Boulders associated to debris flows in this area have a maximum diameter of about 0.5m.

Lyr01 and Lyr28 have extraordinarily long runouts. The debris flows seems to be fairly old, as fully developed vegetation on top was observed. The material of the debris involved in these debris flows is relatively fine with boulders up to 0.3m of diameter.

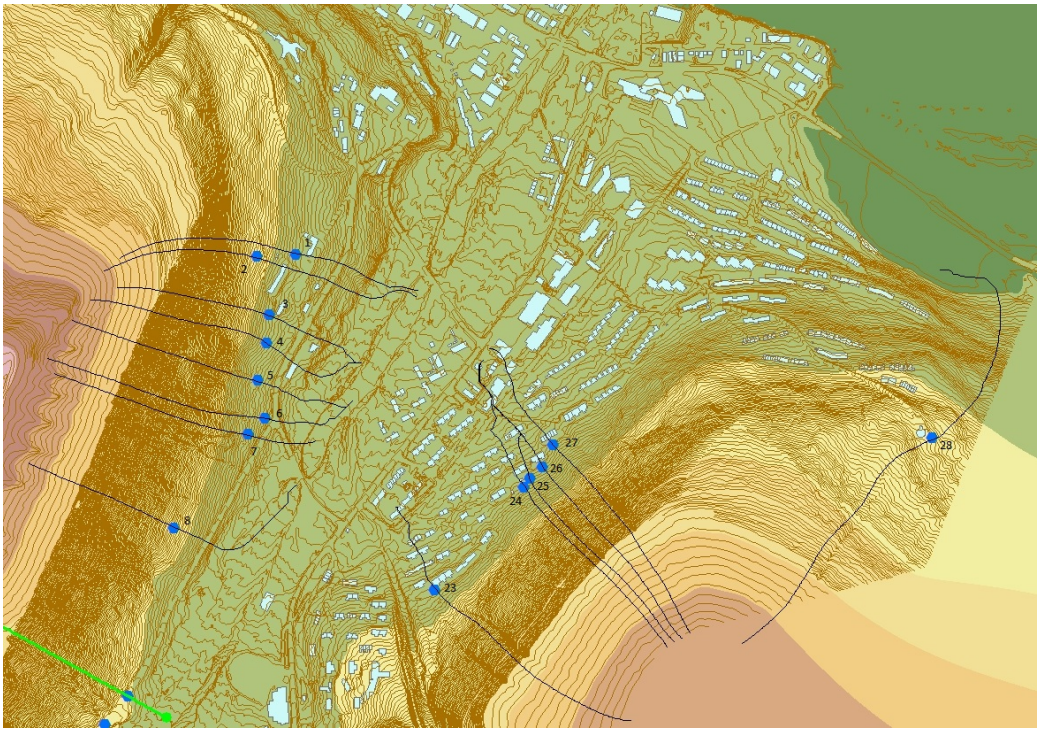

Figure 21: The northern part of Longyeardalen (Picture imported from ArcGIS)

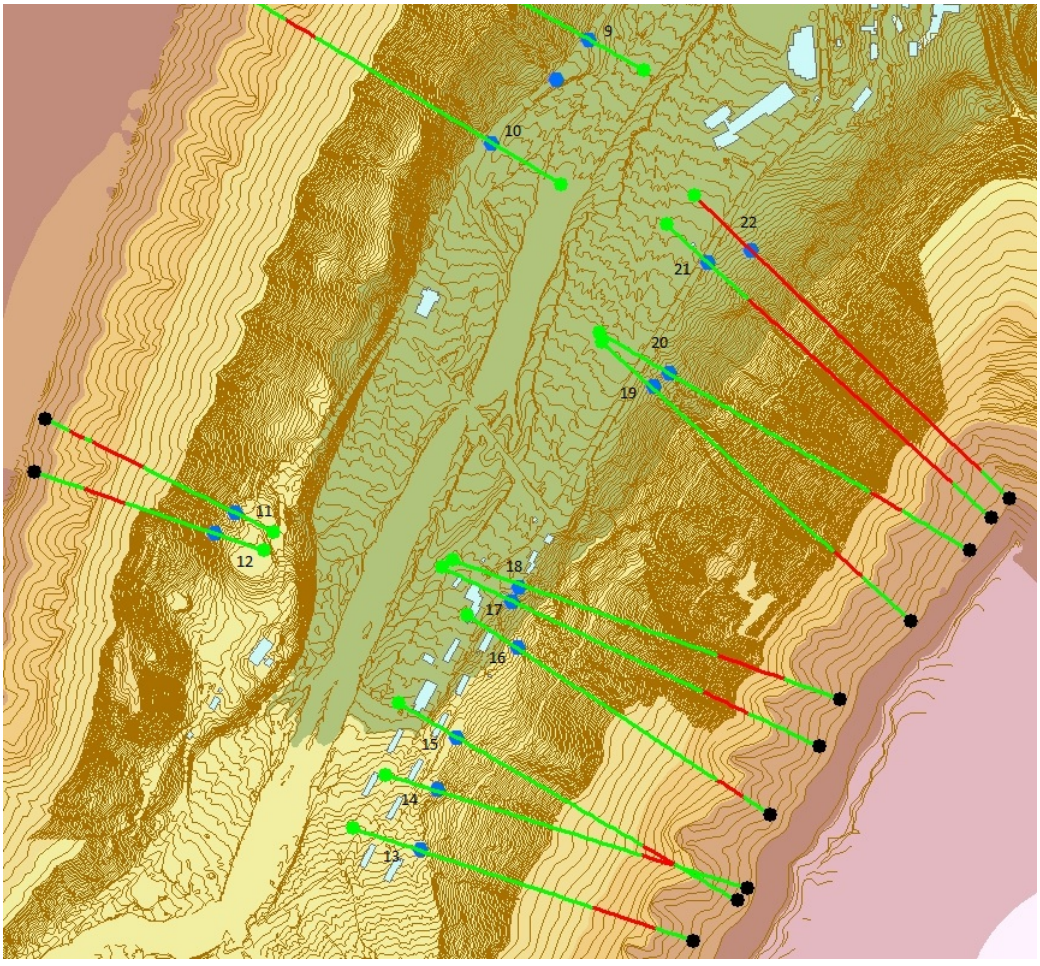

Figure 22: The southern part of Longyeardalen (Picture imported from ArcGIS)

4.1.2 Endalen

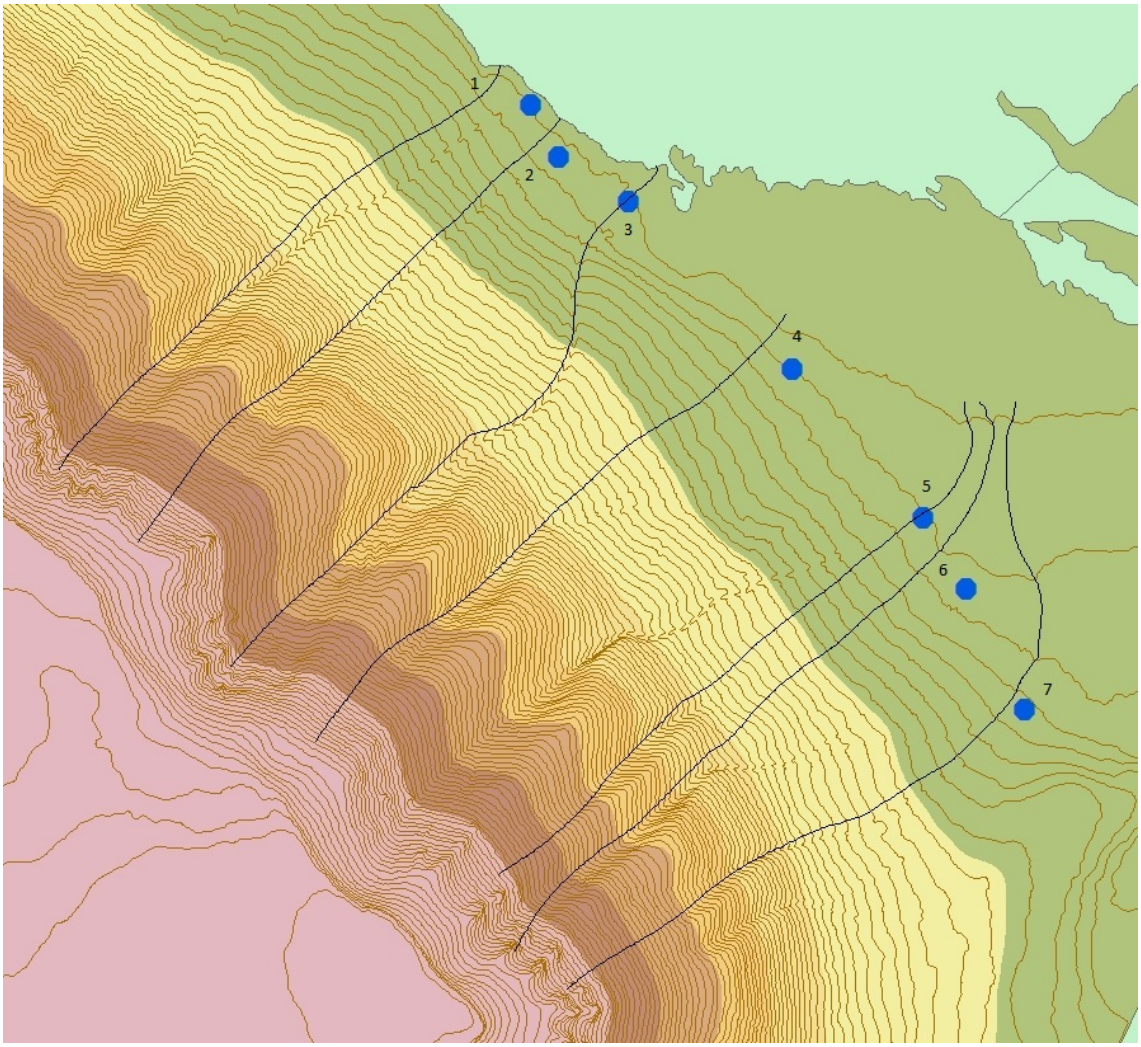

Figure 23: Endalen (Picture imported from ArcGIS)

Fig. 23 shows the results at the outlet of Endalen close to Isdammen. The two debris flows End01 and End02, situated in the northwest of the slope, both superimpose older debris flows, most likely ending in Isdammen.

The debris flows End01 and End02 have a fairly high fraction of stones above 0.10m (70%) and transport boulders up to 1.5m in diameter. The boulders in debris flows End05-07 are smaller. Stones above 0.10m in diameter sum up to 50% of the entire mass within the flow.

4.1.3 Bjørndalen

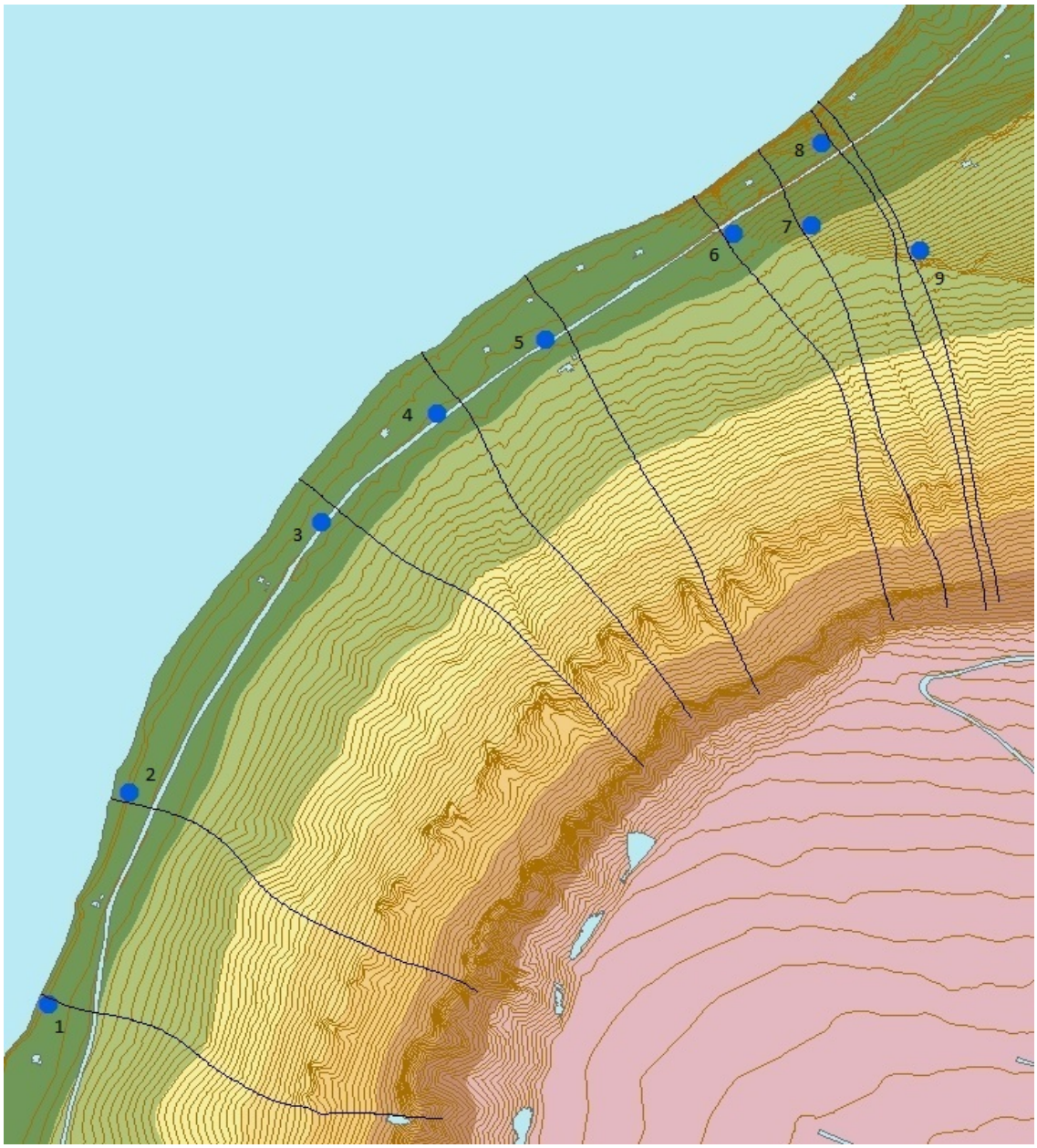

Figure 24: Road to Bjørndalen (Picture imported from ArcGIS)

The survey area close to the road at the seaside between the airport and Bjørndalen included nine debris flows that are relatively old, according to the development of vegetation on top of the debris material. The debris flows Bjo01 and Bjo02 involve a high percentage of big boulders up to 2.0m in diameter. Following the slope to the northeast, the mass fraction of stones above 0.10m and the boulders both become smaller. The debris flows Bjo07-09 involve stones up to only 0.3m in diameter. Bjo08 represents a very old debris flow with an extraordinarily long runout. The runout is about 250m longer than the nearly parallel debris flow runout Bjo09.

4.1.4 Sveagruva

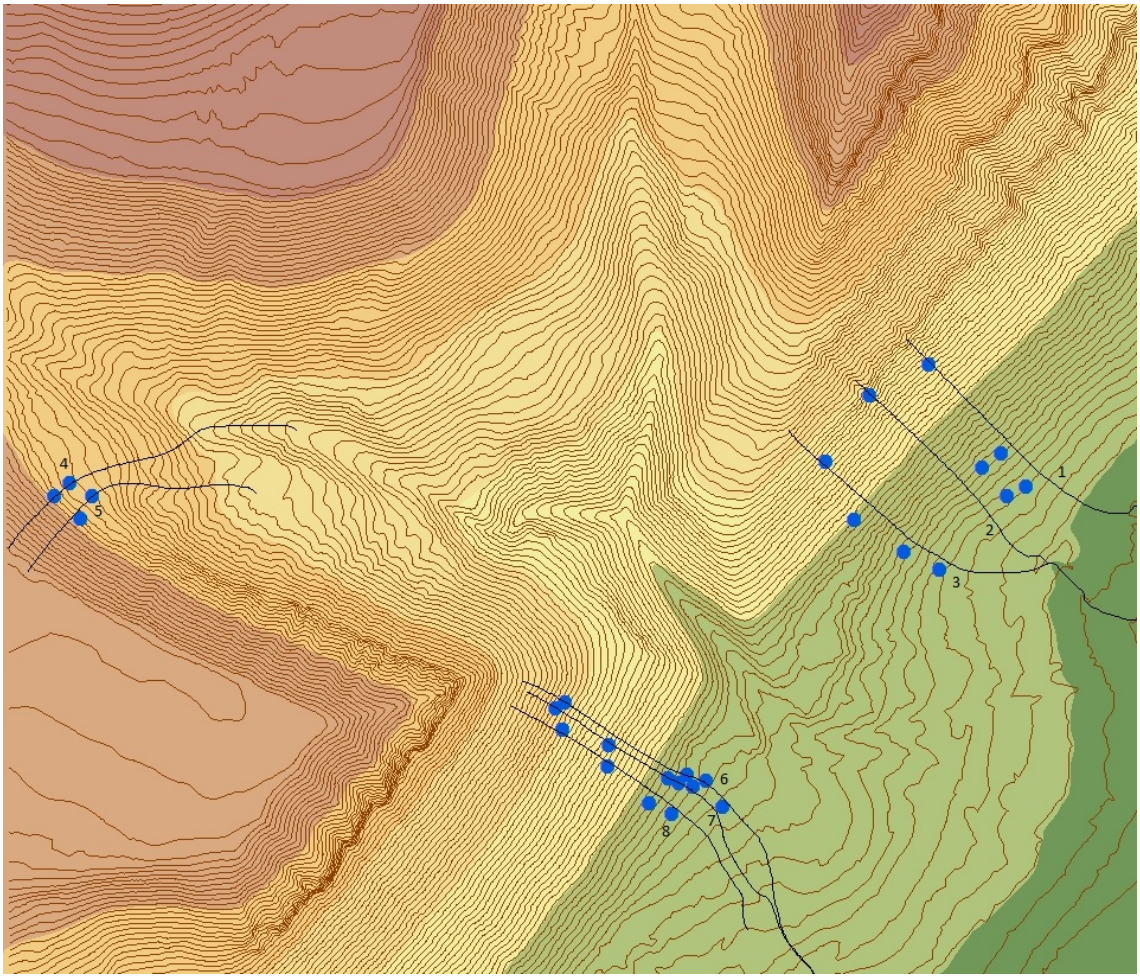

Figure 25: Debris flows in Svea (Picture imported from ArcGIS)

In Svea, several GPS coordinates per profile were taken and are represented by blue points if Fig. 25. The lowest point on each profile corresponds to the maximal runout.

Boulders in the slopes at Sveagruva are up to 1.0m in diameter, while the trenches are at a maximal depth of 1.5m. The mass fraction for material above 0.10m in diameter is around 60% for Sve01-03 and Sve06-08.

Debris flow Sve04 and Sve05 are composed of fine grains with characteristics close to ash. They are the only debris flows of this type observed during the field period.

4.2 Modeling of debris flows

4.2.1 αβ - model and NGI model

Field data acquired during fieldwork and modeling steps described in Chapter 3.3 are compiled into results in Tab. 1-4. As there is good map information about all the research areas, this data is preferred to the slope angles measured with the inclinometer in the field. This is due to the higher accuracy of the map data. This chapter deals with the different regions separately. Results including all valleys and thus all debris flows are shown in Chapter 4.2.2.

An example of results for Longyeardalen of the αβ - model and the NGI model are shown in Tab. 1. For full results, see Tab. 2 in Appendix A.

In the first and second column, the debris flow number and location are given; the third column shows the measured runout angle α, the modeled runout angles $\alpha_{\alpha\beta}$ and α_{NGI} are listed in columns 4 and 6, respectively. The corresponding $\beta_{\alpha\beta}$ and β_{NGI} are listed in columns 5 and 7, respectively; the release slope angle and the slope angle at the maximal runout are noted in the table in columns 8 and 9, respectively.

The table is used to put the modeled slope angles $\alpha_{\alpha\beta}$ and $\alpha_{NGI,}$ via $\beta_{\alpha\beta}$ and $\beta_{NGI,}$ in relation to the measured slope angle α. If the results are within 1.0° deviation from the map data they are marked in green, while results with more than 2.0° deviation are marked in red.

The standard deviation (see Eq. 5) is calculated in order to compare the results.

$$S = \sqrt{S^2} = \sqrt{\frac{1}{n-1}\sum_{i=1}^{n}(X_i - X)^2} \quad (5)$$

Longyeardalen

Table 1: Extract from the results of the αβ - model and the NGI model compared to the slope angle. All slope angles are given in degrees [°].

Debris flow Nr.	Place	Map data	αβ - Model		NGI Model		Release	Runout
		α	$\alpha_{\alpha\beta}$	$\beta_{\alpha\beta}$	α_{NGI}	B_{NGI}	angle	angle
1	Lyr	19,0	18,7	20,9	21,7	26,8	29,2	7,9
2	Lyr	26,7	22,5	24,9	23,3	28,5	30,1	14,2
3	Lyr	24,1	22,8	25,2	23,1	28,3	35,3	7,9
4	Lyr	25,3	23,8	26,2	23,4	28,6	36,2	9,1
5	Lyr	26,6	24,8	27,3	24,2	29,4	35,5	9,1
6	Lyr	25,9	25,1	27,6	25,4	30,6	38,6	8,1

The results show considerable deviation from the measured slope angles and will be discussed in Chapter 5.2. The αβ – model has an average deviation of 2.18°, while the NGI model has an average deviation of 2.13°.

According to equation (5), the standard deviation for the αβ - model is calculated to be 2.5°. The standard deviation calculated for the NGI model is 2.6°.

Endalen

The results in Endalen are shown in Tab. 3 in Appendix A. The results of the αβ - model fit reasonably well with the measured slope angles. Slope angle results have an average deviation of 1.1°.

The results of the NGI model are with 2.2° average deviation somewhat more than in the αβ - model.

The standard deviation for the αβ – model is 1.6° and 2.7° for the NGI model.

Bjørndalen

Tab. 4 in the Appendix A is showing the results for the area close to Bjørndalen. The average deviation is with 1.7°, respectively 2.5° relatively high for both the αβ –model and the NGI model.

The standard deviation for the αβ – model is 2.1° and 3.6° for the NGI model.

Sveagruva

Slope angle modeling results are shown in Tab. 5 in Appendix A. The average deviation is very high, especially for the αβ – model for Svea slopes. The deviation is 4.2° for the αβ – model, while it is 2.7° for the NGI model.

The standard deviation for the αβ – model is 5.0° and 3.1° for the NGI model.

4.2.2 Regression analysis for Svalbard

As explained in Chapter 3.3.3, linear regressions are conducted with the data of the 52 debris flows investigated on Svalbard. The regressions show results for β, defined at a start deposition angle of 10°, 12°, 15° and 20°. The angle β is plotted on the x-axis while α(β) is plotted on the y-axis.

10° model

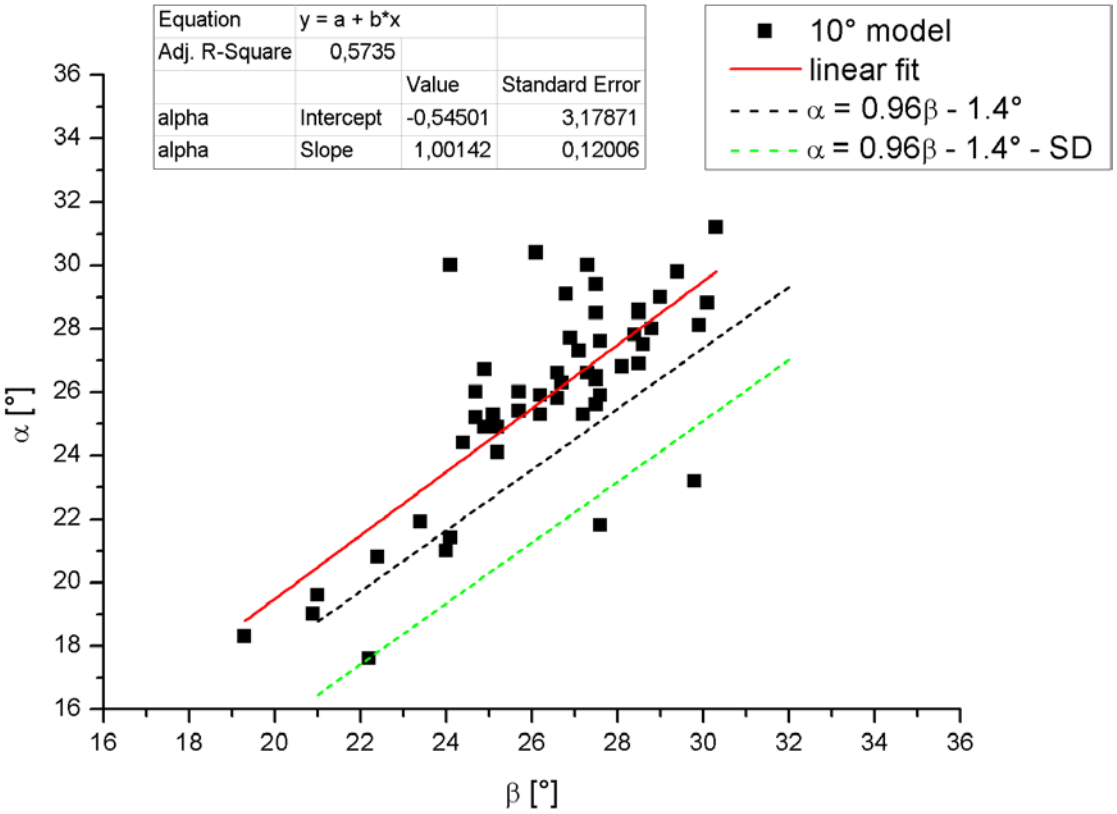

Figure 26: Linear regression with β defined at the slope angle of 10°

Fig. 26 shows a linear regression using all 52 debris flows with β defined at the 10° point. This regression is drafted as a line in red and follows the Equation (6):

$$\alpha = 1.00\beta - 0.55° \quad (6)$$

The standard deviation is 3.18° for the interception and 0.12 for the slope.

In addition, the linear regression for the αβ – model with the mainland Norway data following

$$\alpha = 0.96\beta - 1.4° \quad (2)$$

from Chapter 3.3.1 is drafted with a black dashed line. The green dashed line shows the linear mainland Norway regression with the additional safety criterion of one standard deviation. The αβ – model following Equation (2) has an average deviation of 1.85° to the linear regression of Equation (6) and a standard deviation of 5.03°.

12° model

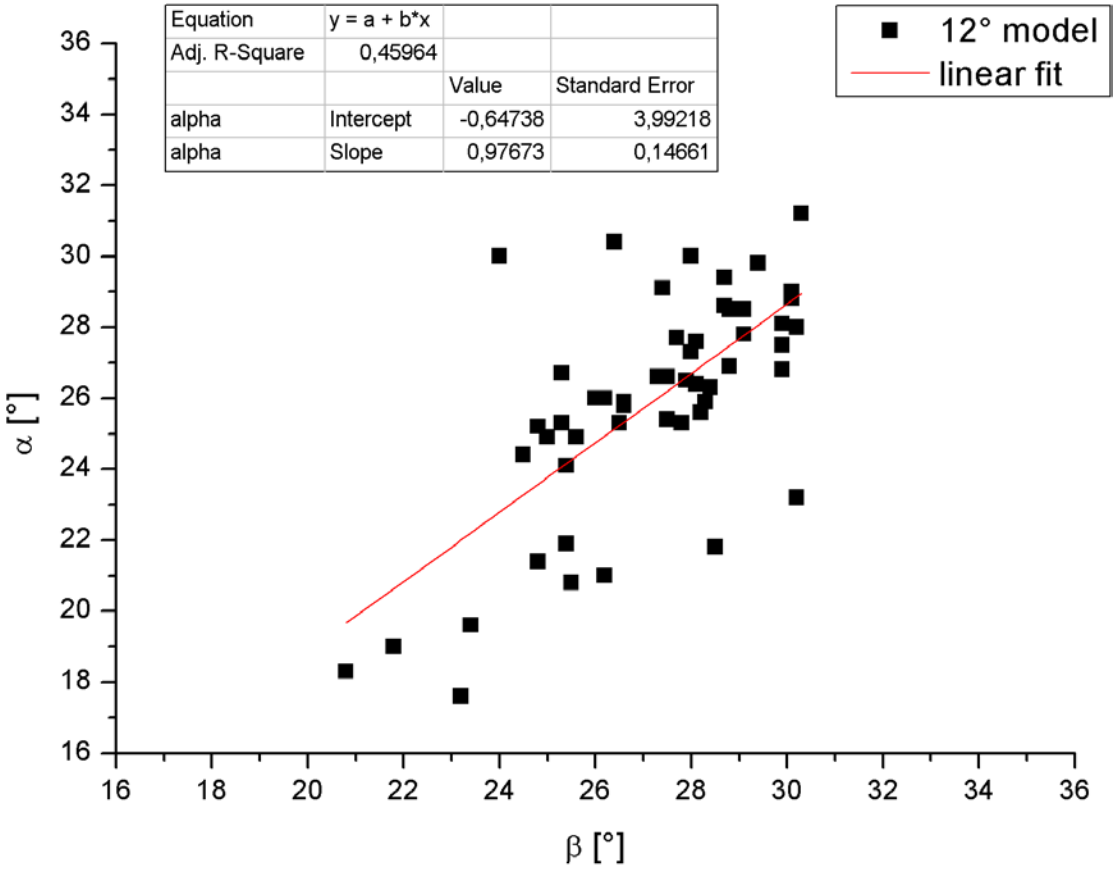

Figure 27: Linear regression with β defined at the slope angle of 12°

Fig. 27 shows a linear regression using all 52 debris flows with β defined at the 12° point. This regression is drafted as a line in red and follows the Equation:

$$\alpha = 0.98\beta - 0.65° \quad (7)$$

The standard deviation is 3.99° for the interception and 0.15 for the slope.

15° model

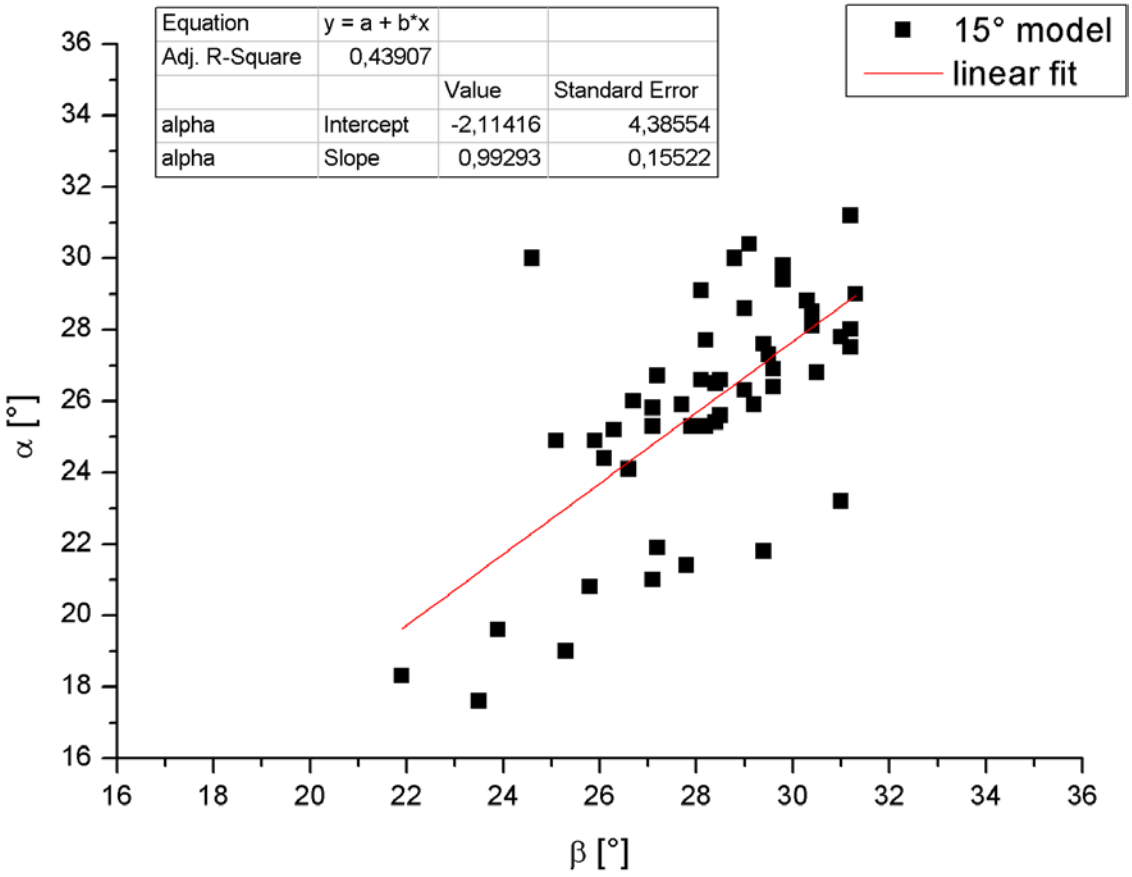

Figure 28: Linear regression with β defined at the slope angle of 15°

Fig. 28 shows a regression using all 52 debris flows with β defined at the 15° point. This regression is drafted as a li0ne in red and follows the Equation:

$$\alpha = 0.99\beta - 2.11° \quad (8)$$

Standard deviation is 4.39° for the interception and 0.16 for the slope.

20° model

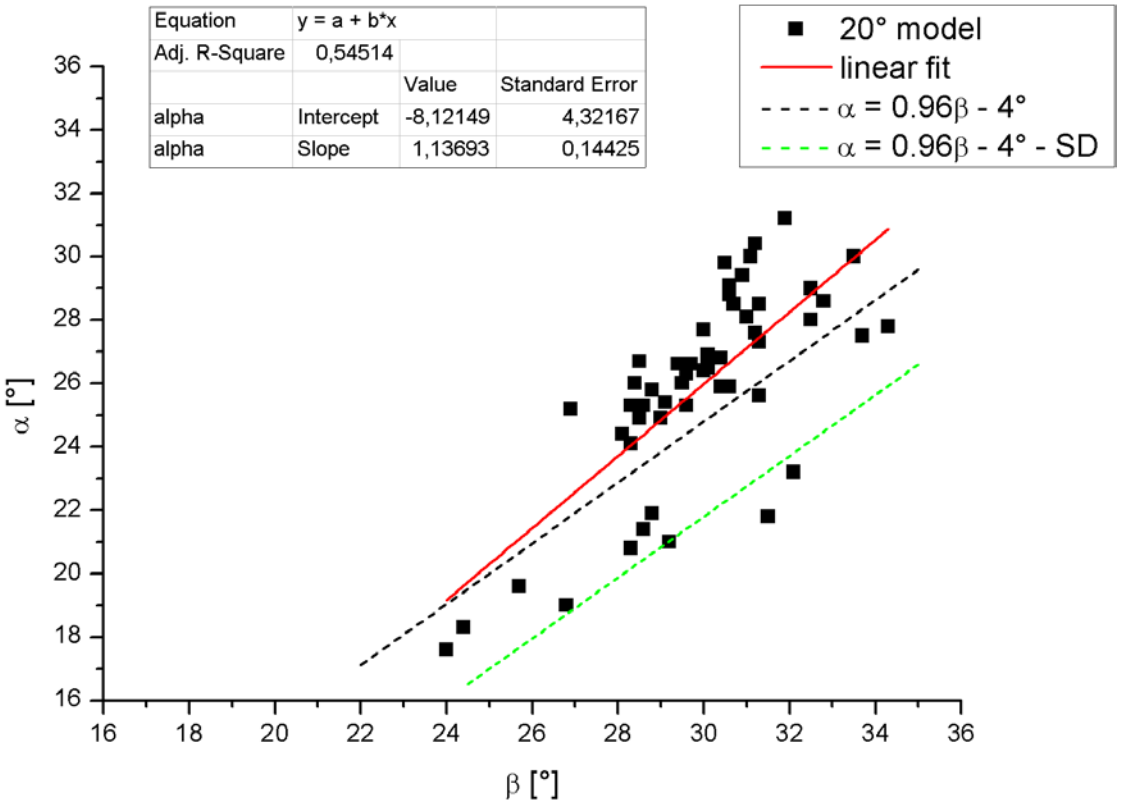

Figure 29: The regression with β at the 10° point. Standard deviation is 3.0°

Fig. 29 shows a regression using all 52 debris flows with β defined at the 20° point. This regression is drafted as a line in red and follows the Equation:

$$\alpha = 1.14\beta - 8.12° \quad (9)$$

Standard deviation is 4.32° for the interception, respectively 0.14 for the slope.

In addition the linear regression for the NGI model with the mainland Norway data following

$$\alpha = 0.96\beta - 4.0° \quad (3)$$

from chapter 3.3.2 is drafted with a black dashed line. The green dashed line shows the linear mainland Norway regression with the additional safety criterion of one standard deviation. The NGI model following Equation (3) has an average deviation of 1.10° to the linear regression of equation (9). This results in a standard deviation of 5.42°.

4.2.3 Extreme runout regressions for Svalbard

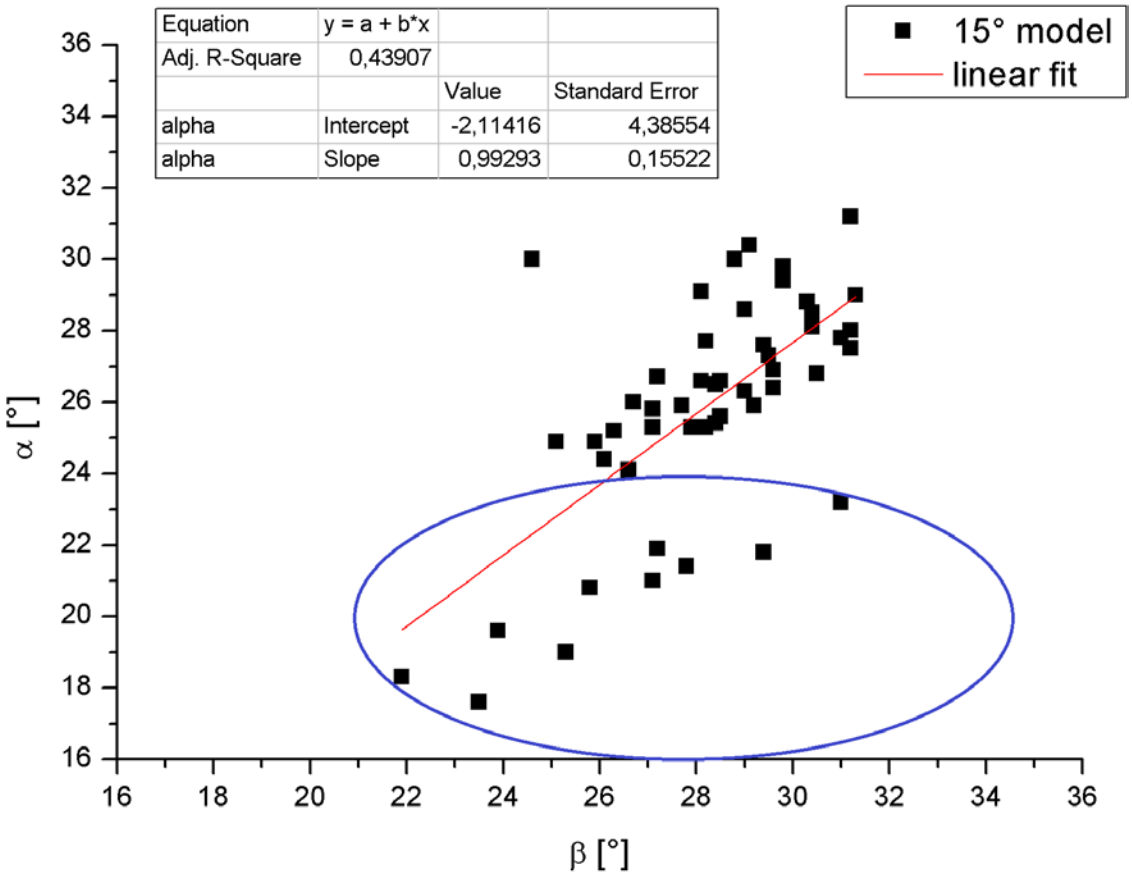

Figure 30: 10 Debris flows with long runouts and thus a small value for the runout angle α

When applying the empirical models from mainland Norway to the Svalbard data, a fairly good fit is found. Yet obviously there are some deviations in the results, showing some of the problems related to modeling. Some debris flow runouts continue onto fairly flat slopes of down to 3.0° steepness, while others stop above 15.0°. This is related to the water content, the type of material involved and other factors described in Chapter 2. It is challenging to fit the same model to all types of debris flow runouts.

For engineering circumstances, the maximal runout, rather than the average runout, is most interesting. Therefore linear regressions including only the lower part of the α–spectrum were executed, see Fig. 33. The linear regressions were calculated for β defined at the 10.0°, 12.0°, 15.0° and 20.0° deposition slope angles. The results are shown in Fig. 34-37.

10° extreme runout model

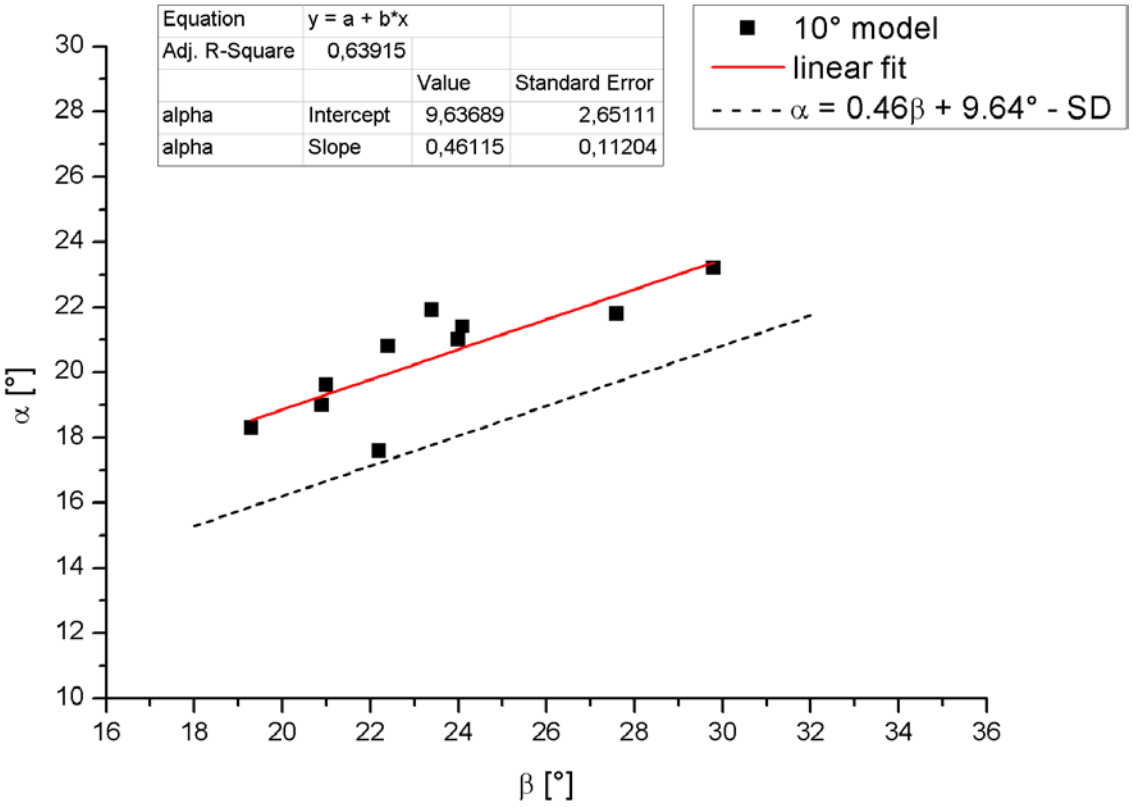

Figure 31: The linear regression with β defined at the slope angle of 10°

Fig. 34 shows a regression using ten very long runouts of debris flows with the 10° slope angle defined as the starting point for deposition. This regression is shown by the red line and has the Equation:

$$\alpha = 0.46\beta + 9.64° \quad (10)$$

The standard deviation is 2.65° for the interception, and 0.11 for the slope.

The black dashed line shows the safety criterion of the Equation (10) minus one standard deviation.

12° extreme runout model

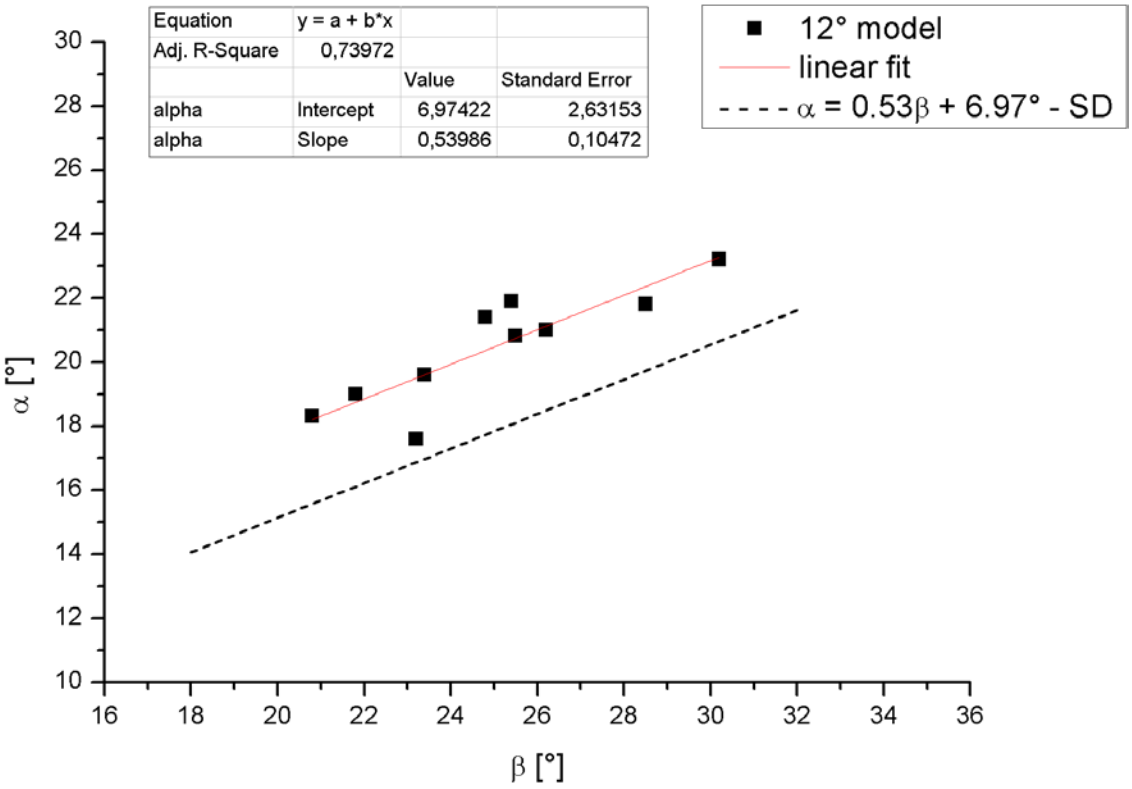

Figure 32: The linear regression with β defined at the slope angle of 12°

Fig. 35 shows a regression using ten very long runouts of debris flows with the 12° slope angle defined as the starting point for deposition. This regression is shown by the red line and has the Equation:

$$\alpha = 0.54\beta + 6.97° \quad (11)$$

The standard deviation is 2.63° for the interception, and 0.10 for the slope.

The black dashed line shows the safety criterion of the Equation (11) minus one standard deviation.

15° extreme runout model

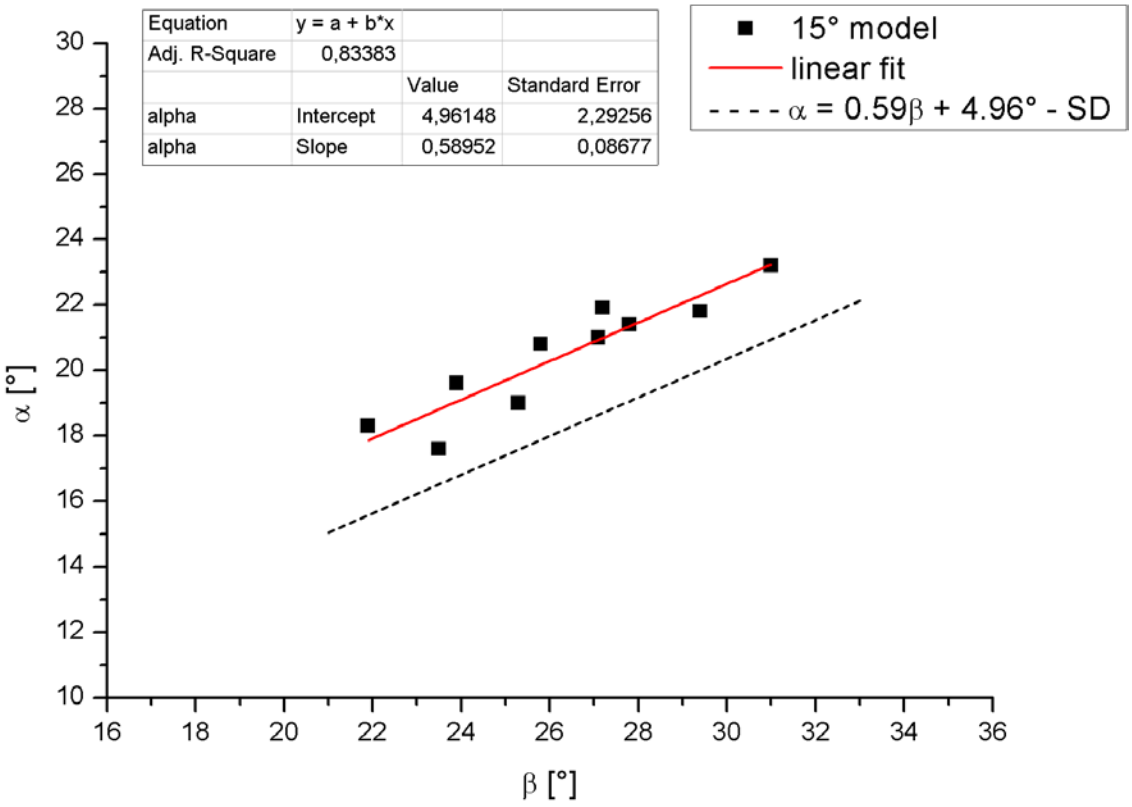

Figure 33: The linear regression with β defined at the slope angle of 15°

Fig. 36 shows a regression using ten very long runouts of debris flows with the 15° slope angle defined as the starting point for deposition. This regression is shown by the red line and has the Equation:

$$\alpha = 0.59\beta + 4.96° \quad (12)$$

The standard deviation is 2.29° for the interception, and 0.08 for the slope.

The black dashed line shows the safety criterion of the Equation (12) minus one standard deviation.

20° extreme runout model

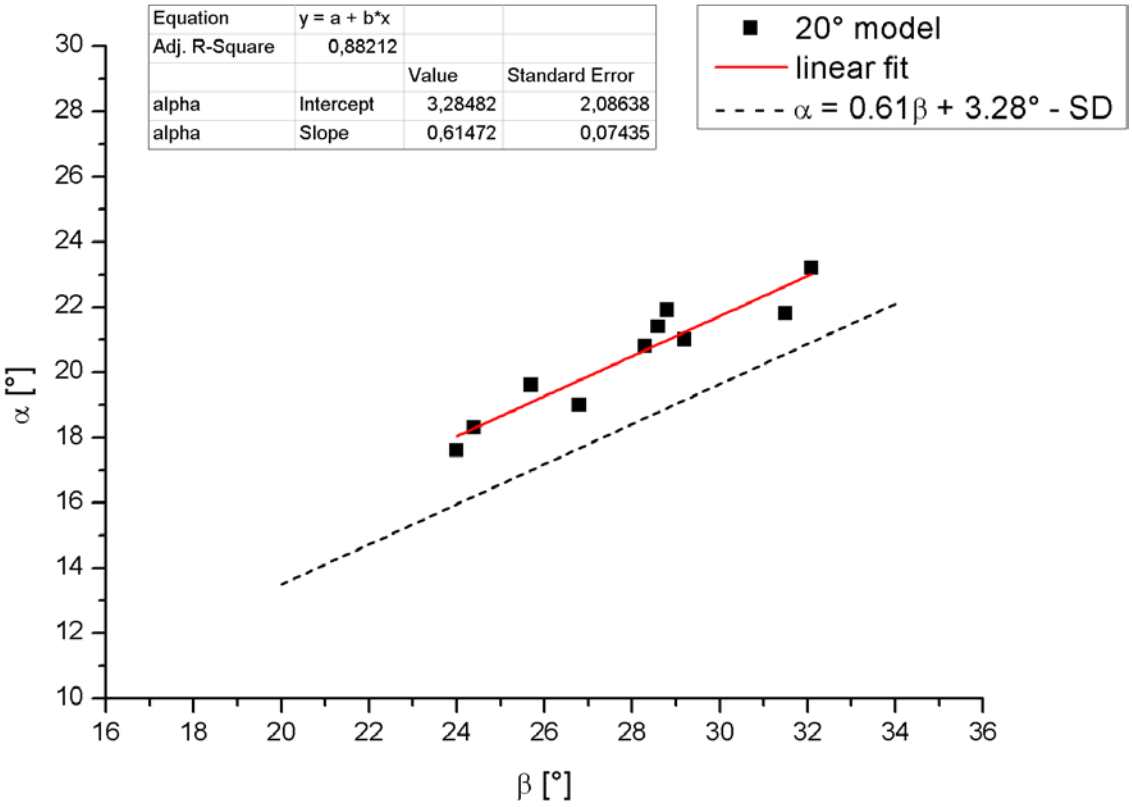

Figure 34: The linear regression with β defined at the slope angle of 20°

Fig. 37 shows a regression using ten very long runouts of debris flows with the 20° slope angle defined as the starting point for deposition. This regression is shown by the red line and has the Equation:

$$\alpha = 0.61\beta + 3.28° \quad (13)$$

The standard deviation is 2.08° for the interception, and 0.07 for the slope.

The black dashed line shows the safety criterion of the Equation (13) minus one standard deviation.

4.3 Dynamical modeling with RAMMS

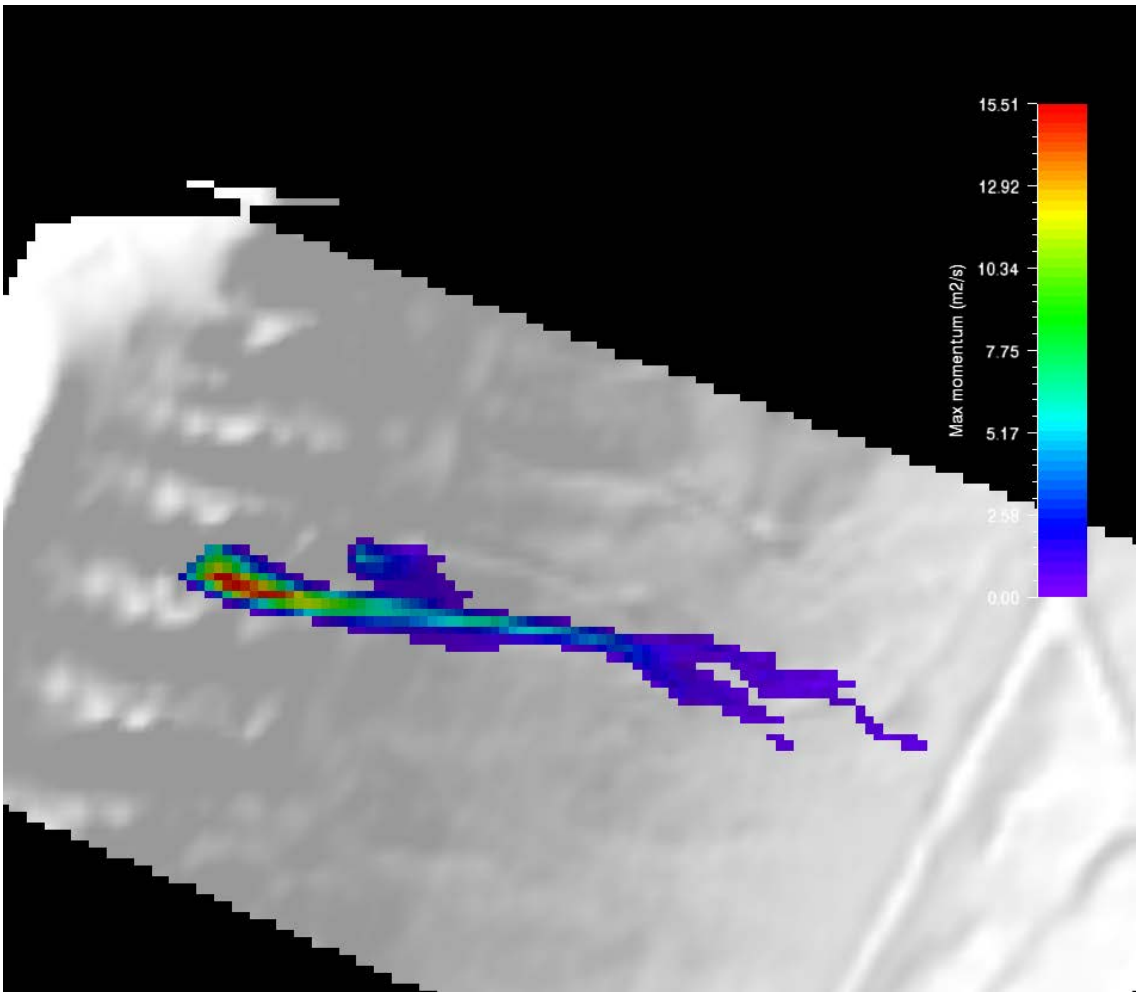

Figure 35: Result of maximum flow momentum for a debris flow located close to Lyr08 with RAMMS Debris Flow

A typical result of RAMMS is shown in Fig. 30. In this case, the maximal flow momentum for debris flow Lyr08 is drafted. The result is valid for a release volume of 800m^3, $\rho = 2{,}000 kg/m^3$, $\mu = 0.14$ and $\xi = 510\ m/s^2$. The release volume is chosen after investigations of Stig Larsson (Larsson 1982). The other values are chosen in a calibration process. A low value for ξ or a high value for μ, tested in calibration, both result in very short runouts.

Reverse modeling was tried for Lyr01-09 and Lyr24-27, as debris volumes were known for those debris flows.

RAMMS in general gives results for the flow height, velocity, the flow momentum and the pressure within the debris flow.

Further results of the modeling are not shown in this paragraph as it has not been possible to calibrate the model considerably well and are later discussed in Chapter 5.3.

Figure 36: Maximal flow height of several possible debris flows at the northwestern outlet of Longyeardalen

The results were exported and shown in ArcGIS map data, see Fig. 31. This example shows possible debris flows in the area of Lyr01-08. Unfortunately only the maximal flow height can be exported as a shape file to ArcGIS. The data for velocity, the flow momentum and the pressure cannot be visualized in ArcGIS.

5 Discussion

This chapter discusses the results and draws connections between mapping data and both empirical and dynamical modeling.

5.1 Field observations

The field investigations have shown some interesting slope characteristics. They seem to be very local, most likely depending on the local geology, geomorphology and/or meteorology. At the outlet of Endalen, for instance, the runout is considerably longer than in Svea. Longyeardalen and Bjørndalen have mixed results.

During field work several generations of debris flows were observed. Debris flows were partly superimposed above old generations of mountain slope hazards. Some debris flows had extraordinarily long runouts compared to neighbor flows and several debris flows were close to present buildings, such as in Nybyen.

Fig. 33 shows a landslide zone map from 2003 for Nybyen. It shows the mountain slope hazard risk for a 1,000 year event with and without the existing buildings. The red line marks the risk zone without existing buildings, while the pink line shows the area exposed to hazards considering the existing first row of buildings. The grey line marks the hazardous area including all existing buildings.

The runouts of the investigated debris flows Lyr13-19 in Nybyen (Fig. 22) were all within the danger zone of Fig. 32 for a 1,000 year event. It is possible, though, that there were larger debris flows in former times that are not visible in the landscape anymore as they might be superimposed by new landscape features.

During the field season there was no occurrence of debris flows in the area around Sveagruva and Longyearbyen. This supports the assumption that debris flows do not occur steadily but as events during, for example, extreme weather conditions.

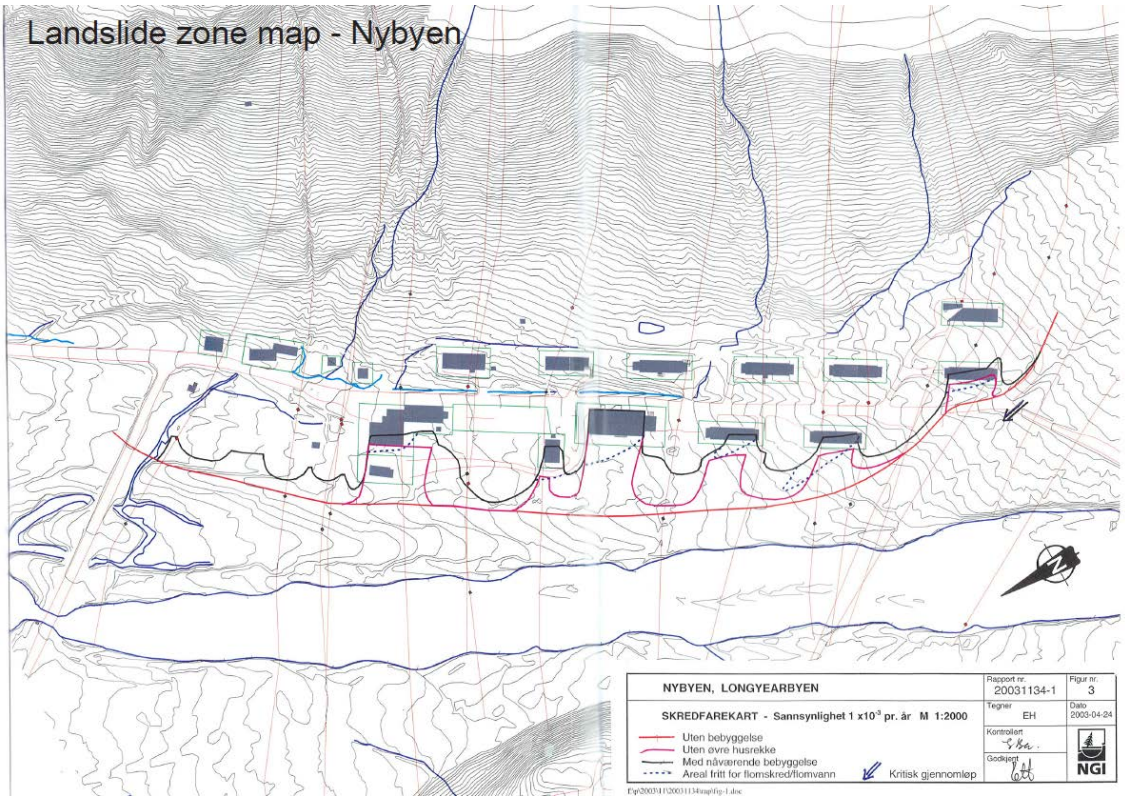

Figure 37: Landslide zone map of Nybyen (NGI 2003). The different lines mark the hazardous area without buildings (red), with the first row of barracks (pink) and considering all buildings (grey).

5.2 Empirical models

The empirical αβ - model and the NGI model both use values measured on debris flows mapped during fieldwork in order to calculate the maximum runouts. Both models are able to illustrate the runout of debris flows relatively well. Taking into account all 52 debris flows, the αβ - model has a standard deviation of 5.03°, while the NGI model has a standard deviation of 5.42°. Generally, the runouts are overestimated by both models. Exceptions are the extraordinary long runouts of Lyr01 (NGI), Lyr28 (αβ), End04-07 (NGI) and Bjo08 (αβ and NGI). The debris flow runouts angle α is underestimated by at least 2.0° for these debris flows.

The overall results are relatively heterogeneous, but homogenous at each field site. Linear regressions fitting to each valley would give considerably better results. As the interest of this study is the whole region, no further work was done on individual valleys.

For improvement of the model, linear regressions have been done, which take Svalbard data into account. For further comparison, different deposition slope angles for the calculation of β have been evaluated. The standard deviation for those models is 3.18°,

3.99°, 4.38° and 4.32° for the 10.0°, 12.0°, 15.0° and 20.0° models. This means that the Svalbard regression for the 10.0° deposition angle is able to predict the runouts most exactly.

Yet, the runout does not completely follow one single linear trend. When analyzing Fig. 27 and Fig. 28 it is evident that debris flows with a runout angle α below 24° show a different behavior than the other debris flows. Whether this fact is due to different weather conditions at the time of occurrence or due to different geomorphology is challenging to answer given the limited amount of data collected.

The geomorphology has an impact on the runout of debris flows. In general, a high content of large boulders results in a shorter runout. Low water content in the soil also generally results in a shorter runout. Fine material however, results in long runout.

The runouts of debris flows in Svea are generally short, which might be explained by the high fraction of large stones and low water content observed during field work. At Haugen and in Endalen, high water content most likely caused the long runouts observed. The high fraction of large stones and short runouts in Bjørndalen and in the southern parts of Longyeardalen are caused by low water content during composition. The considerably long runouts of the debris flows Lyr01, Lyr28 and Bjo8 might be a result of high water content and fine material involved.

These debris flows might also represent 100 year events while the other debris flows represent 20 year events, for instance.

5.3 RAMMS

The results of the dynamical model RAMMS show very short runouts which do not corresponding to the field data. The model was calibrated for 13 different debris flows in Longyeardalen (Lyr01-09; Lyr24-27), but produced runouts that were consistently too short. Longyeardalen was chosen as the modeling field site because release value data from former investigations was available.

The only debris flow that could be accurately described by the model was Lyr08. Former investigations assumed the release debris volume of Lyr08 to be 800m^3. Compared to the other debris flows whose volumes are between 50 m^3 and 300m^3 (Larsson 1982), this is a very large value and probably the reason why Lyr08 is easier to calibrate.

The main problem with the RAMMS model is most likely the fact that the debris flow volumes on Svalbard are very small. The program is not able to process those volumes reasonably. It is designed for considerably higher volumes, see Chapter 3.3.4.

In order to check to what degree the model underestimated the runouts, release areas above the assumed elevation were used. Despite this, the runouts calculated with RAMMS are yet very short.

Although problematic, RAMMS is a very nice tool for visualizing the channeling processes of the debris flows and for gathering information the way the debris flow is going.

5.4 Error sources

Sources of error include the inherent inaccuracies in field data collection due to the human factor, inaccurate models, lack of detailed geomorphological data, small map inaccuracies and calculation mistakes.

For example it is challenging to define the release area of a debris flow in the field. If the release areas are chosen too low on the slope, this leads to high modeled runout angles for α, thus a shorter runout. For instance, a 10.0m height difference for the release area will lead to a 1.25° difference for α for a typical 400.0m long runout and an α around 20.0°.

Considering the fact that the αβ – model, the NGI model and RAMMS are not designed for Svalbard conditions and for higher debris volumes, errors connected to wrong calibration have to be expected.

5.4.1 Empirical models

The empirical models assume that the debris flows start slowing down at a certain point. This point determines β and thus also the runout angle α. The point of slowing down is of course, in reality, different for every avalanche. It might be 20° for one debris flow and 12° for another.

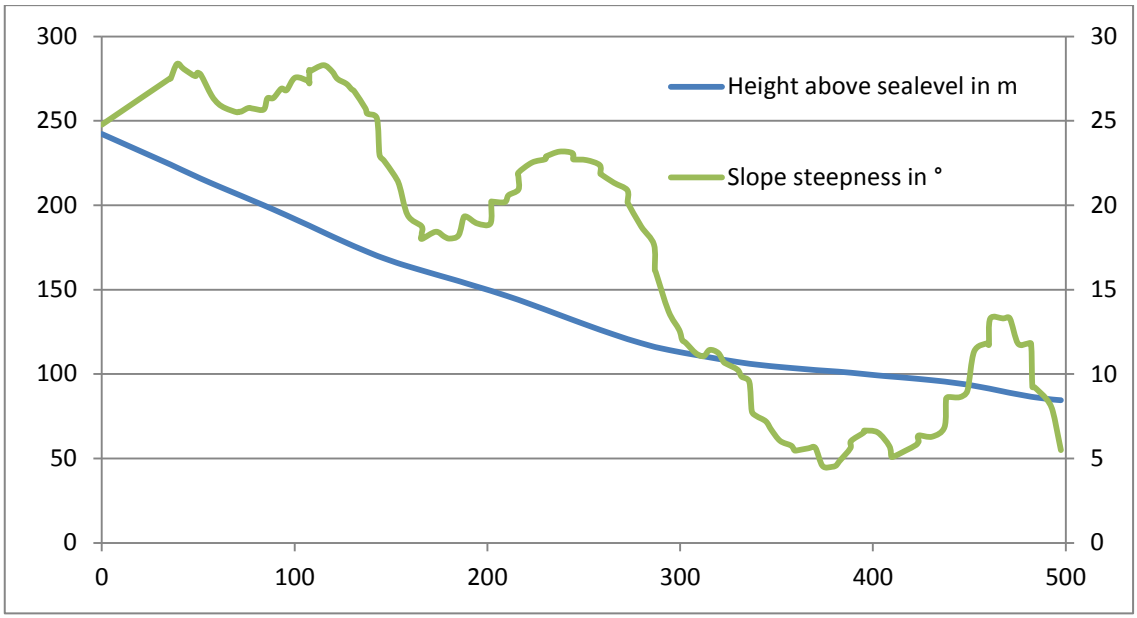

Figure 38: The slope profile of Lyr28 shows that the slope flattens out below 10° at around 330.0m. At around 470.0m the slope profile has 13.0° steepness again.

Single debris flows are challenging to model as they do not follow a uniform concave slope profile. Profiles might go in steps, meaning they flatten out before they get steeper again. In those cases it is hard to use a 10° or 20° slope steepness criteria, see the profile of Lyr28 in Fig. 38.

5.4.2 RAMMS

For successful use of RAMMS, more data about the geomorphology and composition of the debris flows is necessary. One problem is the fact that not enough detailed data about the debris flows was available. Information about the friction coefficients and water content is necessary. Without this data it is very challenging to calibrate the model.

The low debris flow volumes on Svalbard are most likely the largest problem, when using RAMMS as a modeling tool, as the program is calibrated for larger debris flow volumes.

5.5 Comparison of the models

While RAMMS in its current state may be used only for getting an idea about flow directions, empirical modeling can be used for extreme runout predictions on Svalbard. Both the NGI model and αβ – model are showing acceptable results. Taking the stand-

ard deviation into account as a safety margin, both models include all but two debris flow runouts, see Fig. 26 and Fig. 29.

However, the regressions calibrated for Svalbard have a smaller standard deviation and thus better results. The best result is reached by the linear regression in the 10° model with a standard deviation of 3.18°

$$\alpha = 1.00\beta - 0.55° \quad (6)$$

For extreme runouts it is proposed to use the model explained in Chapter 5.2.1 as it only takes into account extraordinary long runouts. The results of those regressions may be used for the engineering purposes at possible construction sites as a high rate of safety is required. The best result within those models is reached by the 20° model leading to the following linear regression

$$\alpha = 0.61\beta + 3.28° \quad (13)$$

with a standard deviation of 2.09°.

All models developed in 5.2.1, include all measured debris flows when applying one standard deviation as a safety criterion.

6 Summary and conclusions

This work focused on empirical and dynamical modeling of debris flow runouts in Svalbard conditions. The aim was to gain further knowledge of the nature of debris flows on Svalbard and the hazards associated to debris flows.

The work included surveys close to two different communities on Svalbard (Longyearbyen and Sveagruva) where in total 52 debris flows were investigated. The results from measurements of the maximum runout were then used in two different empirical models (the αβ – model and the NGI model) and a dynamical model (RAMMS). The models aim to predict the maximum runout of debris flows, which is very important for communities due to safety reasons. Based on the different models and calculations performed, the following conclusions can be made:

- The regressions based on the Svalbard data reach a higher accuracy than the models calibrated on mainland Norway. It is evident that most debris flows on Svalbard have a shorter runout than predicted by the mainland models, but Svalbard debris flows have a higher variation than seen on mainland Norway. This is represented by the larger values for the standard deviation of the Svalbard models. Even though the runout is in general shorter, some of the debris flows have extraordinarily long runouts. The best fit for the surveyed flows is reached by the regression building up on the 10° slope angle deposition criterion. The standard deviation is 3.18° in this case. The regression equation is:
  $\alpha = 1.00\beta - 0.55°$, for β defined at the slope deposition angle of 10°. (6)
- For engineering purposes, models including only the ten longest runouts of the investigations have been used. The model with the 20° slope angle deposition criterion achieved the best result with a standard deviation of 2.09°. This model is advised to use in future construction site planning. The regression equation is:
  $\alpha = 0.61\beta + 3.28°$, for β defined at the slope deposition angle of 20°. (13)
- In general, the output of the αβ – model and the NGI model fit the measured maximal runout.
- Modeling with the dynamical model RAMMS is challenging. The model is a great tool for finding directions of the flow, although the runout is hard to estimate. Reverse modeling of several debris flows in order to calibrate RAMMS was not possible, due to the lack of detailed geomorphological data and the fact that the program is calibrated for different debris flow dimensions.

- High resolution maps are a necessary tool for the survey of debris. If these maps are not available, slope profiles have to be measured manually, which leads to a decrease in accuracy (and a larger uncertainty).
- Most significant sources of errors for modeling are the identification of the release areas, use of models calibrated for other circumstances and simplifications in the models.

6.1 Further work

For complete understanding of the debris flows on Svalbard further work has to be done. Modeling and statistics show that the field data within this work was not sufficient to acquire statistically significant results. More debris flows have to be investigated to get a better understanding of the processes involved. Special focus on geological data about the different slopes is needed. For instance, does different bedrock determine different slope processes in the outlet of Endalen and Longyeardalen? Or might meteorological circumstances or vegetation patterns are the determining factors? Some geological work about debris flows has been done in the 1960s and 1970s (Jahn 1967; Jahn 1976; Glade 2005), but recent data is missing.

Measurements of the composition of fresh debris flows right after their occurrence are of interest as water content of the flow could be measured and lead to better predictions.

It should be investigated to which extent permafrost conditions and climate change are important for debris flows. According to research, continuous permafrost could become discontinuous in some regions in the future (Lewkowicz and Harris 2005). The consequences for the occurrence of debris flows on Svalbard have to be analyzed.

Mountain slope hazards in other Arctic regions like Ellesmere Island in Canada, for instance, have already been investigated (Lewkowicz and Hartshorn 1998). Connecting this work to investigations that have been done on Svalbard would be informative. Comparison to mainland Norway data (Jaedicke et al. 2009) was performed, more detailed future comparisons seem promising.

The models in this work are all dependent on the release area, which is often hard to determine. Therefore it would be interesting to compare models like the ACS model that calculate runout independent of a defined release area.

RAMMS may be an interesting tool for future use. As dynamic models take into account the physics behind the debris flows, they help in understanding the actual processes (Iverson 2006). In the Alps, RAMMS and Elba+ are already used with great success. The field data set is much larger there and the time series are longer.

References

André, M.-F. (1990). Frequency of debris flows and slush avalanches in Spitsbergen: a tentative evaluation from lichenometry. Polish Polar Research 11: 345-363.

Aryal, K. and R. Sandven (2005). Risk evaluation of a slope and mitigation measures: A case study from Nepal. Landslides and Avalanches. I. K. Senneset, K. Flaate and J. O. Larsen, Norge: Taylor & Francis Group.

Bakkehøi, S., U. Domaas and K. Lied (1983). Calculation of snow avalanche runout distance. Annals of Glaciology 4 International Glaciological Society: 24-29.

Broch, E. and B. Nilsen (2001). Ingeniørgeologi - Berg. Trondheim, NTNU.

Caine, M. (1980). The rainfall intensity - duration control of shallow landslides and debris flows. Geografiska Annaler Series A: Physical Geography 62A: 23-27.

Chatwin, S. C., D. E. Howes, J. W. Schwab and D. N. Swanston (1994). A Guide for Management of Landslide-Prone Terrain in the Pacific Northwest: Victoria,

British Columbia. Ministry of Forests.

Christen, M. (2012). Personal communication.

Christiansen, H. H. (2011). Mass movement / Slope processes in periglacial areas. Lecture AG-204. Svalbard, UNIS: p. 53.

Corominas, J. (1996). The angle of reach as mobility index for small and large landslides. Can. Geotech. Journal 33: 260-271.

Dorren, L. K. (2003). A Review of Rockfall Mechanics and Modelling Approaches. Progress in Physical Geography 27(1): 69-87.

Eckerstorfer, M., U. Neumann and H. H. Christiansen (2008). High Arctic avalanche monitoring in maritime Svalbard. International Snow Science Workshop. Whistler.

Elvevold, S., W. Dallmann and D. Blomeier (2007). Svalbards geologi. Tromsø, Norsk Polarinstitutt.

Fannin, J. and E. T. Bowman (2008). Debris flows - entrainment, deposition and travel distance. Geotechnical News 25.

Glade, T. (2005). Linking debris-flow hazard assessments with geomorphology. Geomorphology 66(1): 189-214.

Haid, H. (2007). Mythos Lawine. Eine Kulturgeschichte. Innsbruck, Austria, Studien Verlag.

Highland, L. M. and P. Bobrowsky (2008). The Landslide Handbook - A Guide to Understanding Landslides. Reston, U.S., Geological Survey.

Humlum, O., A. Instanes and J. L. Sollid (2003). Permafrost in Svalbard: a review of research history, climatic background and engineering challenges. Polar Research 22: 191-215.

Hungr, O. (2005). Classification and terminology. Debrisflow Hazards and Related Phenomena. M. Jakob, and Hungr, O. Berlin, Germany, Praxis.

IPCC-AR4-WG1 (2007). Climate Change 2007: The Physical Science Basis, Contribution of Working Group I to the Fourth Assessment Report of the Intergovernmental Panel on Climate Change. S. Solomon, D. Qin, M. Manninget al, Cambridge University Press.

Iverson, R. M. (2006). Forecasting runout of rock and debris avalanches Landslides from Massive Rock Slope Failure. S. G. Evans, G. Scarascia Mugnozza, A. Strom and R. L. Hermanns. Dordrecht, Springer: 197-209.

Jaedicke, C., K. Lied and K. Kronholm (2009). Integrated database for rapid mass movements in Norway. Nat. Hazards Earth Syst. Sci. 9: 469-479.

Jahn, A. (1967). Some features of mass movement on Spitsbergen slopes. Geografiska Annaler Series A: Physical Geography: 213-225.

Jahn, A. (1976). Contemporaneous geomorphological processes in Longyeardalen, Vest-Spitsbergen (Svalbard). Biuletyn Peryglacjalny 26: 253-268.

Larsen, J. O. (2005). The Influence of Climate Change on Natural Hazards in Arctic Region. Landslides and Avalanches. I. K. Senneset, K. Flaate and J. O. Larsen.

Larsson, S. (1982). Geomorphological effects on the slopes of Longyear valley, Spitsbergen, after a heavy rainstorm in July 1972. Geogr. Ann. 64 A: 105-125

Legros, F. (2002). The mobility of long-runout landslides. Engineering Geology. 63: 301-331.

Lewkowicz, A. G. and C. Harris (2005). Frequency and magnitude of active-layer detachment failures in discontinuous and continuous permafrost, northern Canada. Permafrost and Periglacial Processes 16(1): 115-130.

Lewkowicz, A. G. and J. Hartshorn (1998). Terrestrial record of rapid mass movements in the Sawtooth Range, Ellesmere Island, Northwest Territories, Canada. Canadian Journal of Earth Sciences 35(1): 55-64.

Lied, K. and S. Bakkehøi (1980). Empirical calculations of snow-avalanche run-out distance based on topographic parameters. Journal of Glaciology 26(94).

Lied, K. and K. Kristensen (2003). Snøskred: Håndbok om snøskred. Nesbru, I samarbeid med NGI, Norges geotekniske institutt.

McClung, D. and P. Schaerer (2006). The avalanche handbook. Seattle, Wash., Mountaineers Books.

McKnight, T. L. and D. Hess (2000). Climate Zones and Types. Physical Geography: A Landscape Appreciation. Upper Saddle River, NJ, Prentice Hall.

met.no (2012). Norwegian Meteorological Institute. 1961-1990.

NGI (2003). Skredfarekart - Nybyen, Longyearbyen. Rapport Nr. 20031134-1.

NOAA-USGS (2005). NOAA USGS Debris Flow Warning System - Final Report. Reston, Virginia, USA, U.S. Department of the Interior: 60.

Norem, H. and F. Andersen (2011). Flom- og sørpeskred - Håndbok om sikring av veger som er utsatt for vannrelaterte skred - Håndbok 284.

Pedersen, M. B. and Ø. S. Hellum (2007). En sammenstilling av grunnundersøkelser i Longyearbyen. Prosjektrapport NTNU.

Prick, A., M. Guglielmin and A. Strini (2004). Rock weathering in Central Spitsbergen and in Northern Victoria Land (Antarctica). The Annals of the Marie Curie Fellowshil 3: 50-55.

Prochaska, A. B., P. M. Santi, J. D. Higgins and S. H. Cannon (2008). Debris-flow runout predictions based on the average channel slope (ACS). Engineering Geology 98: 29-40.

RAMMS (2011). User Manual. P. Bartelt, Y. Buehler, M. Christenet al, WSL Institute for Snow and Avalanche Research SLF. 1.4 Debris Flow.

Reynolds, J. M. (1992). The identification and mitigation of glacier-related hazards: examples from the Cordillera Blanca, Peru. Geohazards. G. J. H. McCall, D. J. C. Laming and S. C. Scott, Chapman & Hall, London (1992) 143–157.

Rickenmann, D. (2005). Runout prediction methods. Debris-Flow Hazards and Related Phenomena. M. Jakob and O. Hungr. Heidelberg, Praxis-Springer: 263-282.

Solomon, S., D. Qin, M. Manning, Z. Chan, M. Magquis, K. B. Averyt, M. Tignor and H. L. Miller (2007). Climate Change 2007: The Physical Science Basis. Contribution of Working Group I to the Fourth Assessment Report of the Intergovernmental Panel on Climate Change. New York.

Takahashi, T. (2007). Debris flow: mechanics, prediction and countermeasures. London, Taylor & Francis.

TopoSvalbard (2012). From http://toposvalbard.npolar.no/. Accessed on the 21.03.2012.

VanDine, D. F. (1996). Debris flow control structures for forest engineering: Victoria, British Columbia, Canada. Ministry of Forests Reseach Program.

Weather data from: http://www.climate-charts.com and http://www.wunderground.com

Wieczorek, G. F. and T. Glade (2005). Climatic factors influencing occurence of debris flows. Debris-flow Hazards and Related Phenomena. O. Hungr and M. Jakob, and Hungr, O. Berlin, Germany, Springer Berlin Heidelberg.

Åkerman, J. (1980). Studies on periglacial geomorphology in West Spitsbergen. Lunds Univ. Geogr. Inst. Ser. Avh. 89. Medd. Lund, Sweden.

List of figures

List of tables

Appendix

A Tables

Longyeardalen

Table 2: Results of the αβ-model and the NGI model compared to the slope angle α. Slope angles are given in degrees [°]. Red highlighted cells mark deviations above 2.0° between modeled and mapped α; green cells accord to deviations below 1.0°.

Debris flow Nr.	Place	Map data	αβ - Model		NGI Model		Release	Runout
		α	$\alpha_{\alpha\beta}$	$\beta_{\alpha\beta}$	α_{NGI}	B_{NGI}	angle	Angle
1	Lyr	19,0	18,7	20,9	21,7	26,8	29,2	7,9
2	Lyr	26,7	22,5	24,9	23,3	28,5	30,1	14,2
3	Lyr	24,1	22,8	25,2	23,1	28,3	35,3	7,9
4	Lyr	25,3	23,8	26,2	23,4	28,6	36,2	9,1
5	Lyr	26,6	24,8	27,3	24,2	29,4	35,5	9,1
6	Lyr	25,9	25,1	27,6	25,4	30,6	38,6	8,1
7	Lyr	27,3	24,6	27,1	26,1	31,3	38,9	10,6
8	Lyr	30,4	23,6	26,1	26,0	31,2	38,6	17,1
9	Lyr	25,8	24,1	26,6	23,6	28,8	34,0	5,6
10	Lyr	28,8	27,5	30,1	25,4	30,6	35,1	4,0
11	Lyr	31,2	27,7	30,3	26,6	31,9	38,9	14,1
12	Lyr	29,8	26,8	29,4	25,3	30,5	42,1	14,3
13	Lyr	24,9	22,8	25,2	23,4	28,5	36,8	6,9
14	Lyr	25,2	22,3	24,7	21,8	26,9	33,1	13,2
15	Lyr	24,4	22,1	24,4	22,9	28,1	34,6	9,0
16	Lyr	26,0	22,3	24,7	24,3	29,5	34,5	12,6
17	Lyr	25,3	22,7	25,1	23,2	28,3	36,0	12,6
18	Lyr	24,9	22,5	24,9	23,8	29,0	39,2	11,9
19	Lyr	26,0	23,3	25,7	23,3	28,4	38,1	12,0
20	Lyr	25,9	25,1	27,7	25,2	30,4	36,3	15,2
21	Lyr	25,6	25,0	27,5	26,0	31,3	40,0	6,3
22	Lyr	28,5	26,0	28,5	25,5	30,7	35,7	10,0
23	Lyr	25,3	24,7	27,2	24,4	29,6	26,6	6,7
24	Lyr	26,9	25,9	28,5	24,9	30,1	29,4	9,4
25	Lyr	26,4	25,0	27,5	24,8	30,0	28,6	6,9
26	Lyr	26,3	24,2	26,7	24,4	29,6	28,3	7,9
27	Lyr	25,4	23,3	25,7	23,9	29,1	32,4	8,3
28	Lyr	17,6	19,9	22,2	19,0	24,0	24,8	7,5

Endalen

Table 3: Endalen. Results of the αβ - model and the NGI model compared to the slope angle α. All slope angles are given in degrees [°]. Red highlighted cells mark deviations above 2.0° between modeled and mapped α; green highlighted cells accord to deviations below 1.0°.

Debris flow Nr.	Place	Map data	αβ - Model		NGI Model	
		α	$\alpha_{\alpha\beta}$	$\beta_{\alpha\beta}$	α_{NGI}	B_{NGI}
1	End	19,6	18,8	21,0	20,7	25,7
2	End	21,9	21,0	23,4	23,6	28,8
3	End	18,3	17,2	19,3	19,4	24,4
4	End	20,8	20,1	22,4	23,1	28,3
5	End	21,0	21,6	24,0	24,0	29,2
6	End	21,4	21,7	24,1	23,5	28,6
7	End	21,8	25,1	27,6	26,3	31,5

Bjørndalen

Table 4: Bjørndalen. Results of the αβ - model and the NGI model compared to the slope angle α. All slope angles are given in degrees [°]. Red highlighted cells mark deviations above 2.0° between modeled and mapped α; green highlighted cells accord to deviations below 1.0°.

Debris flow Nr.	Place	Map data	αβ - Model		NGI Model	
		α	$\alpha_{\alpha\beta}$	$\beta_{\alpha\beta}$	α_{NGI}	B_{NGI}
1	Bjo	28,6	25,9	21,5	27,5	32,8
2	Bjo	28,1	27,3	29,9	25,7	31,0
3	Bjo	26,5	25,0	27,5	24,9	30,1
4	Bjo	26,8	25,6	28,1	25,2	30,4
5	Bjo	27,8	25,8	28,4	29,0	34,3
6	Bjo	26,6	24,1	26,6	24,5	29,7
7	Bjo	28,0	26,2	28,8	27,2	32,5
8	Bjo	23,2	27,2	29,8	26,8	32,1
9	Bjo	27,5	26,1	28,6	28,4	33,7

Sveagruva

Table 5: Svea. Results of the αβ - model and the NGI model compared to the slope angle α. All slope angles are given in degrees [°].Red highlighted cells mark deviations above 2.0° between modeled and mapped α; green highlighted cells accord to deviations below 1.0°.

Debris flow Nr.	Place	Map data	αβ - Model		NGI Model	
		α	$\alpha_{\alpha\beta}$	$\beta_{\alpha\beta}$	α_{NGI}	B_{NGI}
1	**Sve**	27,7	24,4	26,9	24,8	30,0
2	**Sve**	29,4	25,0	27,5	25,6	30,9
3	**Sve**	29,1	24,3	26,8	25,4	30,6
4	**Sve**	29,0	26,4	29,0	27,2	32,5
5	**Sve**	30,0	21,7	24,1	28,2	33,5
6	**Sve**	28,5	25,0	27,5	26,0	31,3
7	**Sve**	27,6	25,1	27,6	26,0	31,2
8	**Sve**	30,0	24,8	27,3	25,9	31,1

B Pictures

Longyeardalen

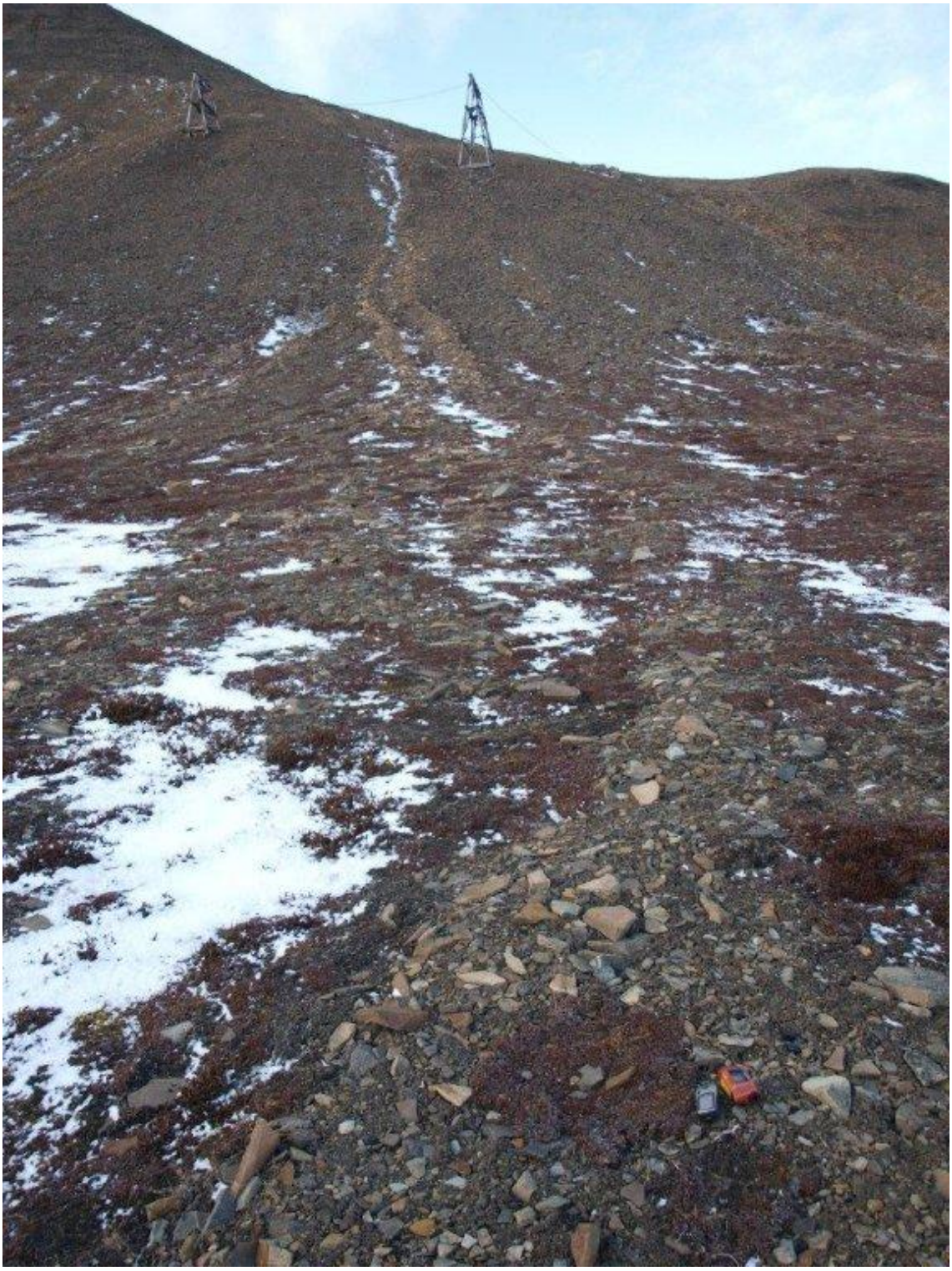

Figure 39: Debris flow Lyr02

Figure 40: Debris flow Lyr09

Figure 41: Material of debris flow Lyr09 in detail

Figure 42: Debris flow Lyr14

Figure 43: Debris flow Lyr15 in detail

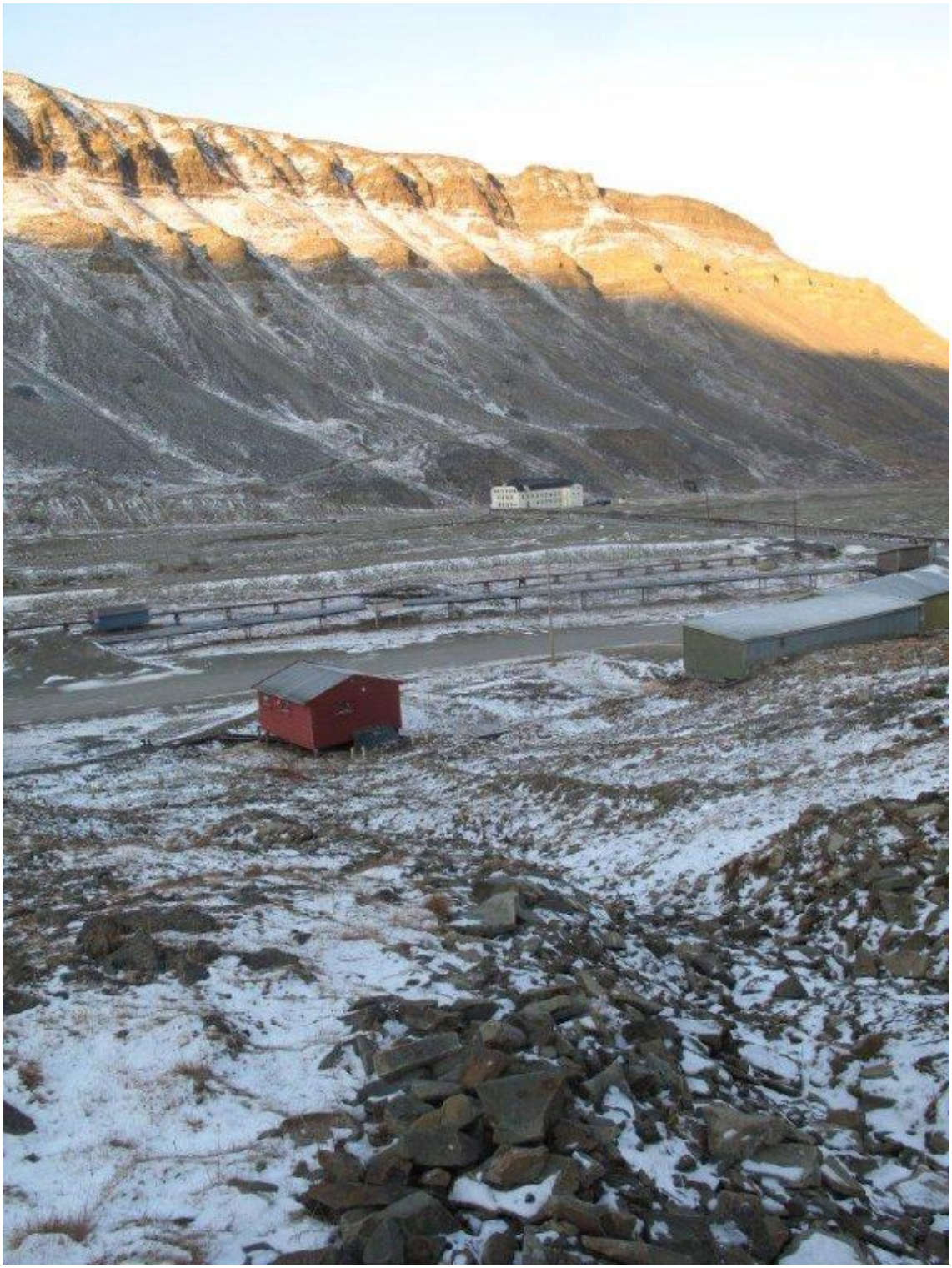

Figure 44: Debris flow Lyr17

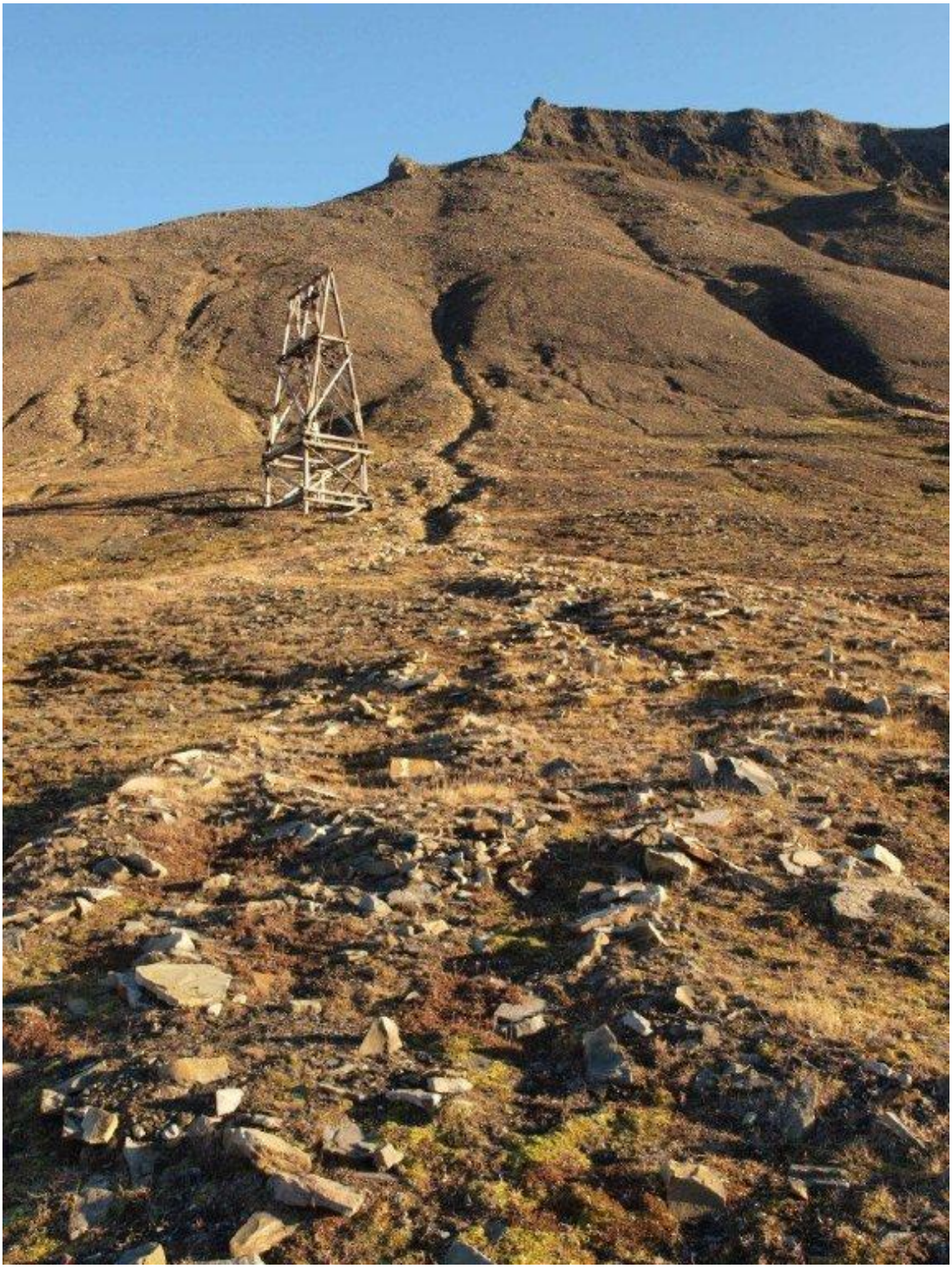

Figure 45: Debris flow Lyr21

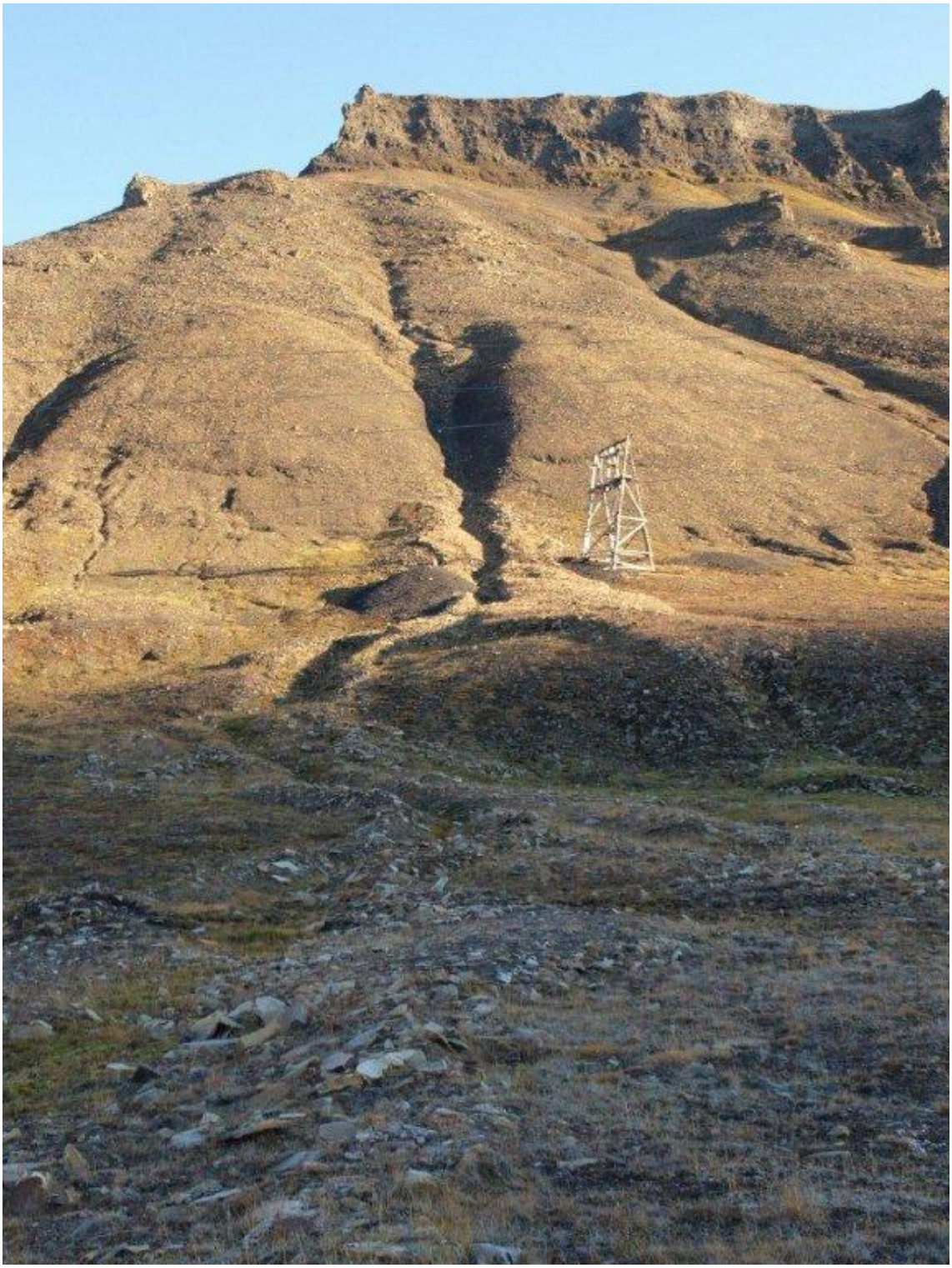

Figure 46: Debris flow Lyr22

Figure 47: Runout of debris flow Lyr23

Figure 48: Triggering zone of debris flow Lyr26

Endalen

Figure 49: Release area of debris flow End05

Figure 50: Runout of Debris flow End01

Bjørndalen

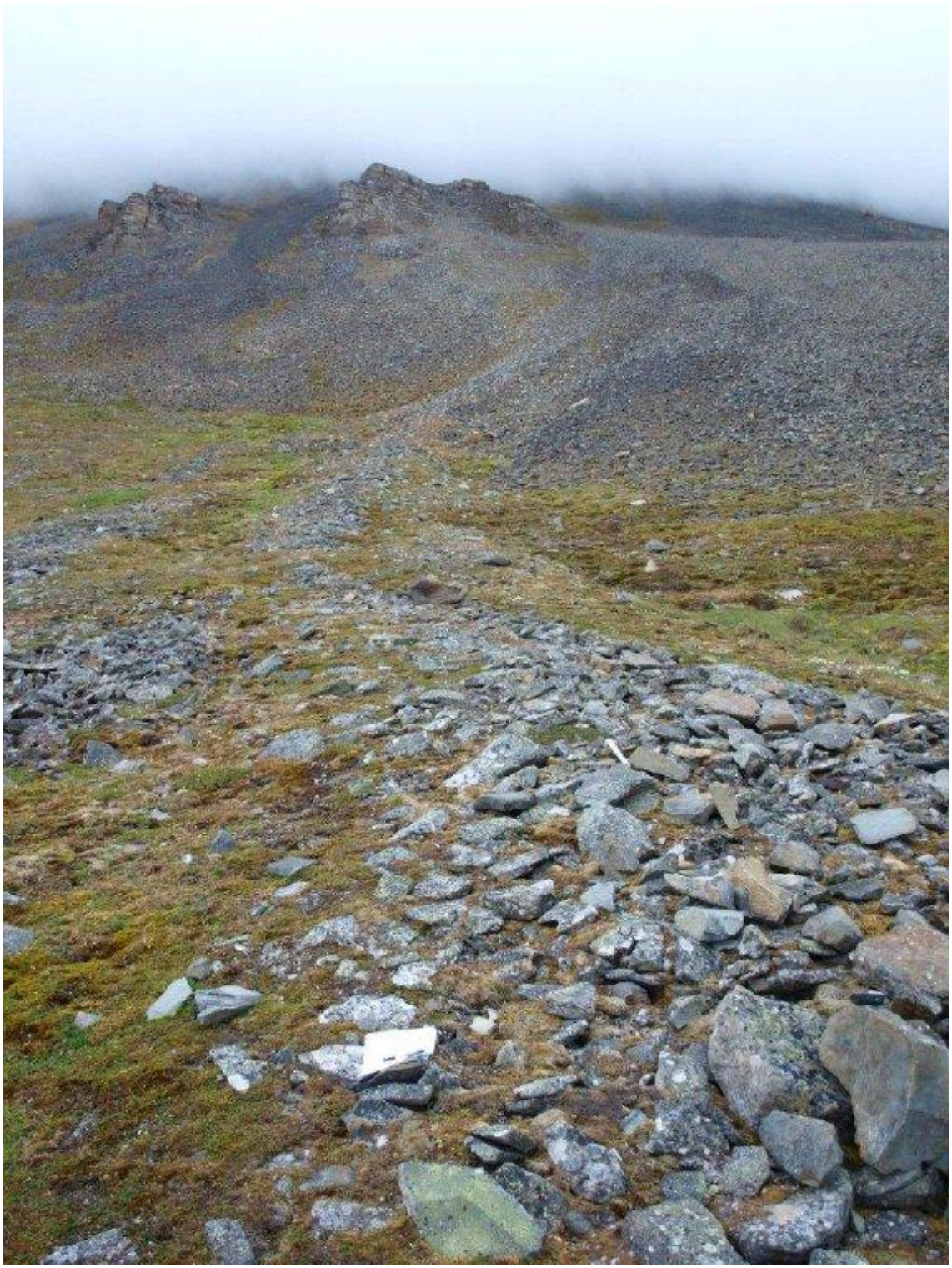

Figure 51: Debris flow Bjo01

Figure 52: Runout of debris flow Bjo02 directly to the sea

Figure 53: Runout of debris flow Bjo04

Figure 54: Runout of debris flow Bjo05

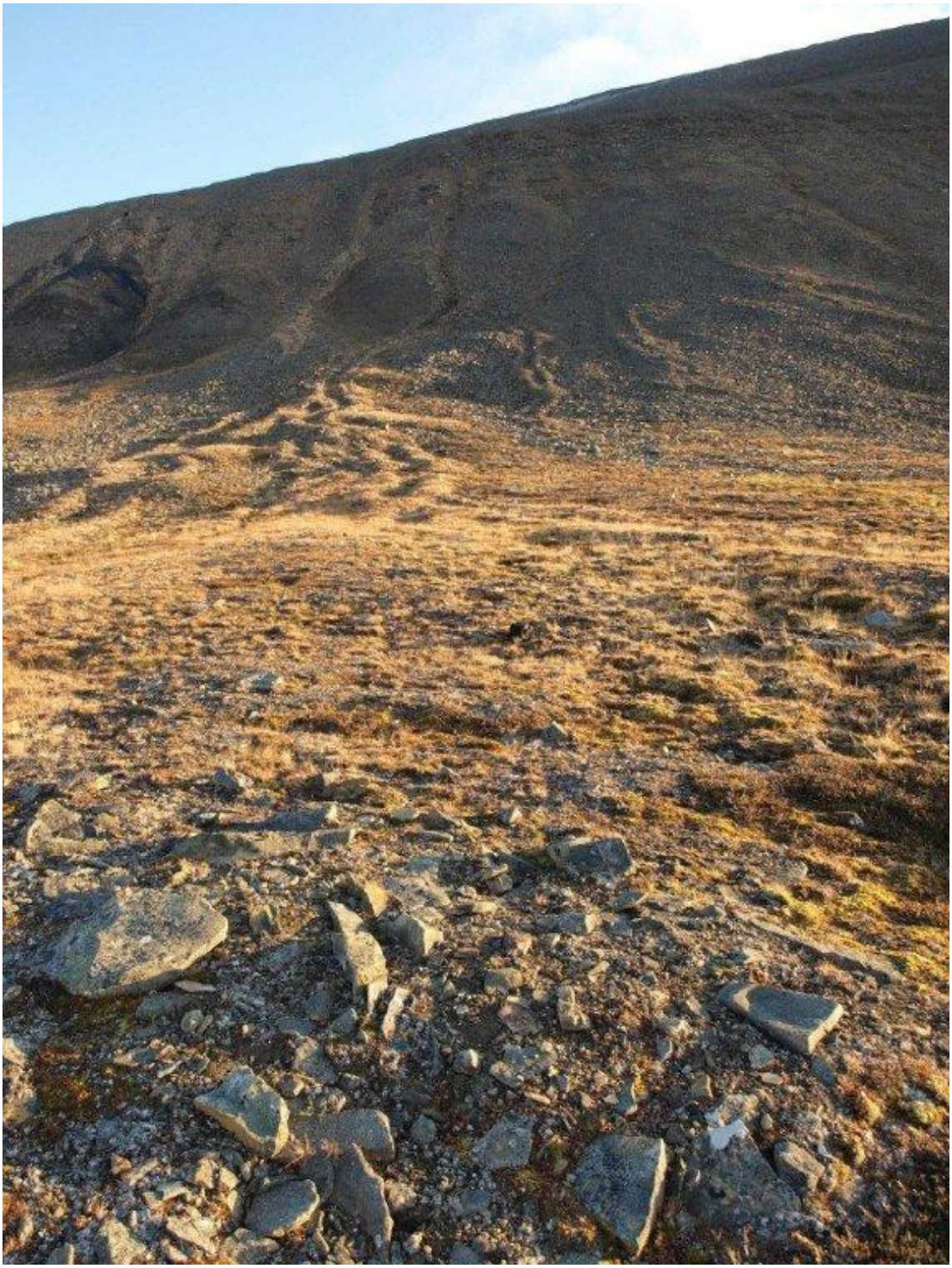

Figure 55: Debris flow Bjo06 (to the right) and Bjo07 (to the left)

Sveagruva

Figure 56: Release area of Sve02

Figure 57: Runout of Sve02

Figure 58: Debris flows on the south side of Braganzavågen, close to Sveagruva. This might be the object for further investigations.